

ENT

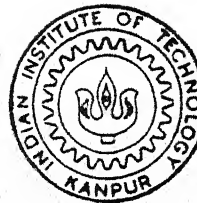
COMPUTATION OF FLOW OVER DELTA WINGS

by

CHETAN KUMAR

TH
AE/1994/M
K96c

TH
629-132322
K96c



DEPARTMENT OF AEROSPACE ENGINEERING
INDIAN INSTITUTE OF TECHNOLOGY KANPUR
MAY, 1994

AE
1994
M
KUMAR
COM



COMPUTATION OF FLOW OVER DELTA WINGS

*A Thesis Submitted
in Partial Fulfillment of the Requirements
for the Degree of*

MASTER OF TECHNOLOGY

by
CHETAN KUMAR

to the
**DEPARTMENT OF AEROSPACE ENGINEERING
INDIAN INSTITUTE OF TECHNOLOGY
KANPUR**

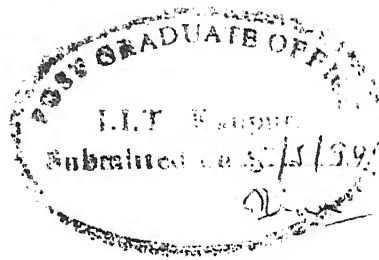
MAY, 1994

AE-1994-M-CHE-COM

TR
620.132322
K 034

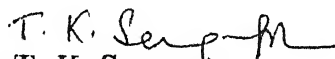
26 MAY 1994/AE
CENTRAL LIBRARY
I. I. T., KANPUR

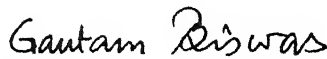
Inv. No. A. 117800



Certificate

It is certified that the work contained in the thesis entitled "*Computation of Flow over Delta Wings*", by Chetan Kumar, has been carried out under our supervision and that this work has not been submitted elsewhere for a degree.


Dr. T. K. Sengupta
Dept. of Aerospace Engineering
Indian Institute of Technology
Kanpur


Dr. Gautam Biswas
Dept. of Mechanical Engineering
Indian Institute of Technology,
Kanpur

Abstract

The present study has been undertaken to investigate the incompressible flow field about a sharp edged delta wing at high angles of attack. The interest in the high angle of attack aerodynamics to improve the performance of fighter aircraft in sharp and sudden maneuvers leads one towards delta wings. Delta wings are not only not stalled at such high angles of attack but they also produce more lift (non linear or vortex lift) due to the separation of flow at the leading edges which takes the form of a pair of vortices on the upper surface. High angles of attack are encountered not only in such extraordinary situations (like dog fighting) but also during landing and take-off. The reason why delta wings are used in fighter aircraft is also related to the wave drag experienced in supersonic flight which can be reduced if the wings are sharp edged and highly swept in addition to the slender configuration of the fuselage itself. Though the supersonic flight is expected for fighters where delta wings find application we are considering only subsonic case.

The flow about a sharp edged delta wing has been obtained by solving the full Navier-Stokes equations. Marker-and-Cell (MAC) algorithm of Harlow and Welch (1965) has been used for the solution. The convective terms have been discretized using a hybrid scheme between first order upwind and second order central differencing. Central differencing has been used for viscous terms. The vortex structure has been obtained and coefficients of pressure at different axial locations have been found out. A grid refinement effort was undertaken for which convergence could not be obtained. Validation of the results could not be accomplished.

Acknowledgements

I take this opportunity to express my deep gratitude , regards and thanks to my thesis supervisors Dr. T. K. Sengupta and Dr. G. Biswas. I was specially fortunate to have enjoyed a lot of freedom during the course of this work both in choosing the problem and trying to solve it which took me many a times in directions which did not really help. But all this has proved to be a great learning experience in more than one way.

I am also thankful to friends M. T. Nair, P. Deb, A. K. Saha for helping me in this work. Also, acknowledgements are due to many other friends who have made my stay at the institute a memorable one.

Chetan Kumar

Nomenclature

AR	aspect ratio of the wing
C_p	coefficient of pressure
$C_{r,c}$	root chord of the wing
P	nondimensional static pressure normalized by ρU_∞^2
Re	Reynolds number (based on the root chord of the wing)
t	nondimensional time
U,V,W	axial, normal and transverse components of velocity (nondimensional)
U_∞	free stream velocity
X,Y,Z	axial, normal and transverse dimension of coordinates (normalized by C_r)

Greek Symbols

α	angle of attack
Δ	divergence of flow field
ν	kinematic viscosity
ρ	density

subscripts, suprescripts and indices

i, j, k	index for axial, normal and transverse components of variables
ia, ja	X- and Y-direction indices for the apex of the wing
ib, jb	X- and Y-direction indices for the trailing edge of the wing
kh	Z-direction index for the apex
iim, jim, kim	maximum number of grid points in X-, Y- and Z-direction respective
n	superscript for time level

Contents

1	Introduction	1
1.1	General	1
1.2	Flow Field	2
1.3	Delta and Related Configurations	6
1.4	Scope of the Present Work	8
2	Review of Literature	10
3	Mathematical Formulation	16
3.1	Introduction	16
3.2	Statement of the Problem	16
3.2.1	Governing Equations	16
3.2.2	Grid	17
3.2.3	Boundary Conditions	18
3.3	Discretization of the Equations	23
3.3.1	Continuity Equation	23
3.3.2	Momentum Equations	23
3.4	Marker-and-Cell Method	24
3.4.1	Salient Features	24
3.4.2	Computational Scheme	26
3.4.3	Pressure-Velocity Iteration	27
3.4.4	Stability Criteria	30
4	Results and Discussions	32
4.1	Velocity vectors	32
4.2	Pressure Distribution	33
4.3	Vorticity Contours	34

List of Figures

1.1	Vortex flow about delta wing	4
1.2	Pressure distribution and lift coefficient on a slender delta wing . . .	4
1.3	Top view of the breakdown of the leading edge vortices on a delta wing (Werle 1960)	5
3.1	Grid spacing in the computational domain	18
3.2	Three dimensional staggered grid with relative location of the variables	19
3.3	Relative location of the velocities and the wing surface (XY plane) .	19
3.4	Velocity boundary conditions on the wing	20
3.5	U-components on the wing surface	21
3.6	W-components on the wing surface	22
4.1	Cross-stream velocity vectors at different axial locations ($\alpha = 20.5$) .	35
4.2	Cross-stream velocity vectors at different axial locations ($\alpha = 25$) . .	36
4.3	Cross-stream velocity vectors at different axial locations ($\alpha = 30$) . .	37
4.4	Cross-stream velocity vectors at different axial locations ($\alpha = 35$) . .	38
4.5	Cross-stream velocity vectors at different axial locations ($\alpha = 40$) . .	39
4.6	Pressure contours at different axial locations ($\alpha = 20.5$)	40
4.7	Pressure contours at different axial locations ($\alpha = 25$)	41
4.8	Pressure contours at different axial locations ($\alpha = 30$)	42
4.9	Pressure contours at different axial locations ($\alpha = 35$)	43
4.10	Pressure contours at different axial locations ($\alpha = 40$)	44
4.11	Coefficient of pressure distribution ($\alpha = 20.5$)	45
4.12	Coefficient of pressure distribution ($\alpha = 25$)	46
4.13	Coefficient of pressure distribution ($\alpha = 30$)	47
4.14	Coefficient of pressure distribution ($\alpha = 35$)	48
4.15	Coefficient of pressure distribution ($\alpha = 40$)	49
4.16	Vortex breakdown on Delta Wing (computational results) ($\alpha = 60$) .	50
4.17	Vorticity contour (Re = 1000)	51

Chapter 1

Introduction

1.1 General

Agility and supermaneuverability are two concepts which are being increasingly talked about in connection with design of modern combat airplanes and tactical missiles. These relate to the performance of airplanes and missiles in close air combat and laser guided smart missiles. Agility refers to the sharp maneuvering of the flight vehicle. Supermaneuverability attempts to utilize regions of the maneuver envelope that have been unattainable historically such as post stall flight maneuver and side-slipping. With these factors in mind the first thing to be looked into are the lifting surfaces or the wings. The wings should give forces and moments for that extra edge in close air combat. Wings for these applications necessarily have to be different from conventional rectangular wings which experience stalling at angles of attack near 15-17 degrees. Delta wings come into picture which have been long known to be effective beyond this upper limit of conventional wing configurations. Also, it has been long known that fighter aircraft flying at high speeds need to have thin profile and sharp edges with wings triangular or delta planform..

1.2 Flow Field

The features of the flow observed about delta wings have been extensively described in the literature. Based primarily on the experimental studies by Legendre(1952), Earnshaw(1962), Wentz & McMahon(1966), Fink & Taylor(1967), Fink(1956) and Hummel(1979) the flow field has been firmly established.

For a finite span wing the pressure difference between the upper and the lower surfaces makes the flow three-dimensional as cross flow velocities are induced on the surfaces. These cross flow velocities cause the air to flow around the wing tip from the lower ("pressure") side to the upper ("suction") side. This results in the shedding of vorticity and the formation of trailing vortices. Due to the velocity induced due to the vorticity content of the shear layer it tends to roll up into tip vortex as it develops. This kind of separation occurs in all finite span wings. The strength of the shed vortex is increased if the wing is swept back. Delta wing is the limiting case of such increase in the angle of sweep. As suggested by Rehbach (1973) one way to visualize the flow over a slender delta wing is to consider the flow established on a deformed slender rectangular wing as its leading edge span is deformed to zero span, i.e. a pointed nose. The final stage of this deformation is delta wing where the two sides of the slender rectangular wing becomes the leading edges of the triangular wing. The vortices are shed from these leading edges of the triangular wing.

Under influence of the vorticity contained in it, the free shear rolls up in a spiral fashion to form a relatively compact single-branched core with distributed vorticity, the so called leading edge vortex core (fig. 1.1). The presence of this core in the promixity of the wing surface affects the pressure distribution on the wing to a large

extent,

the predominant effect being a low pressure region underneath the position of the vortex core (Fig. 1.2). It is the low-pressure region that is responsible for the increment in the lift due to the vortex flow, the so-called vortex lift or non-linear lift. As the angle of attack is decreased, or the leading-edge sweep is decreased, the vortex system becomes weaker, smaller and closer to the wing surface resulting in a suction peak that is lower and narrower, i.e. sharper. It has been observed in experiments that the adverse pressure gradient in the region just outboard of the lateral position of the center of the leading-edge vortex causes a so-called secondary separation. The free shear layer emanating smoothly at the line of secondary separation rolls up in a vortex core also.

At increasing angles of attack, the induced lift forces due to these vortices increase as long as the strength of the rolled-up vortices continue to increase. At angles of attack above certain value the leading edge vortices are known to experience the phenomenon of vortex breakdown or vortex burst. This phenomenon is characterised by a sudden deceleration of the axial flow in the vortex core and increase in the circumferential velocity associated with the rapid expansion of the vortex core. The increase of the nonlinear lift is diminished when the bursting of the concentrated vortices moves over the wing surface, so that the further increase of the angle of attack will accelerate the effect of "vortex breakdown" until the wing stalls. Thus the performance of the delta wing suffers above the angle of vortex burst. This affects the aerodynamic and stability characteristics of the wing adversely.

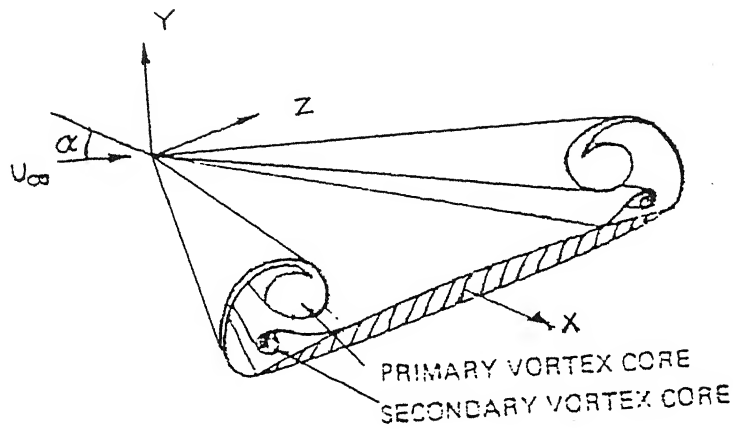


Figure 1.1: Vortex flow about delta wing

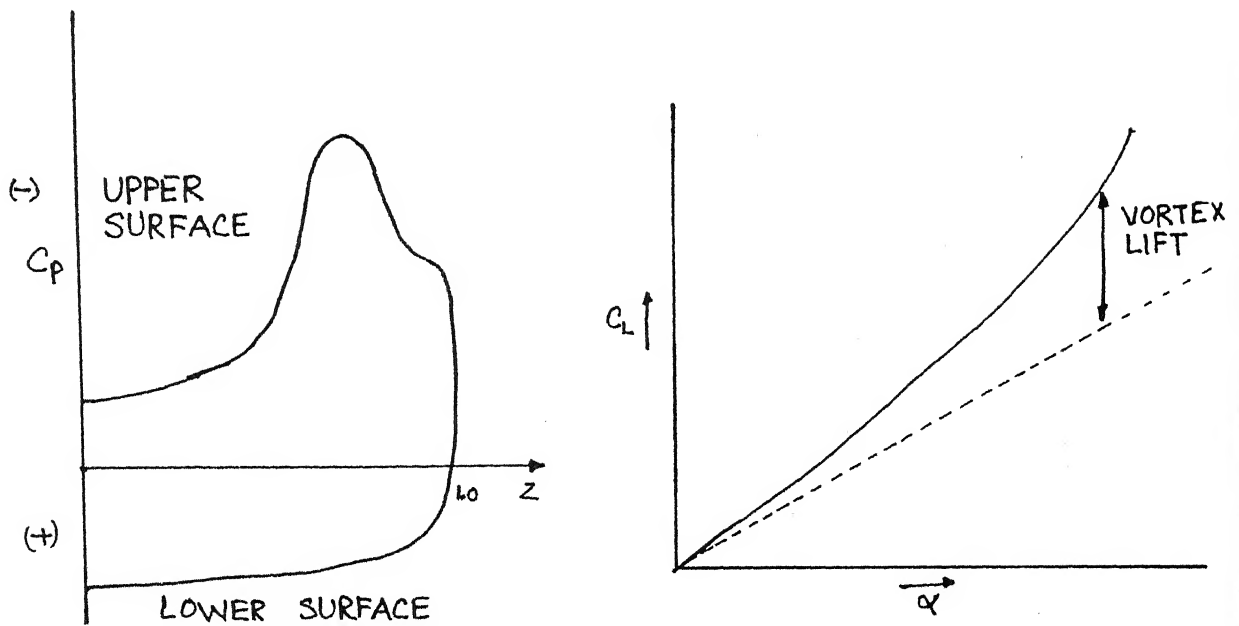


Figure 1.2: Pressure distribution and lift coefficient on a slender delta wing

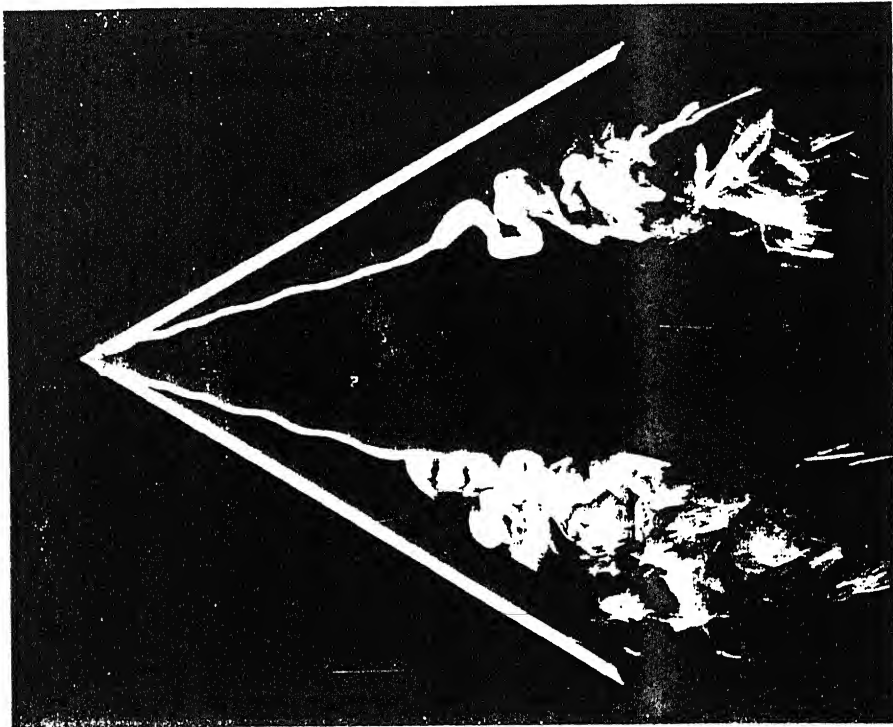


Figure 1.3: Top view of the breakdown of the leading edge vortices on a delta wing (Werle 1960)

1.3 Delta and Related Configurations

The delta wing has been used in various aircraft not as "pure" delta wing but in some derived forms. The reason for this is that the vortex system can be made to resist breakdown and strength can be augmented by certain ways. Though no effort has been made in this study to consider these variations but these warrant mention for the sake of having a perspective of the application.

Improved aerodynamic performance of delta wing configuration at high angles of attack can be achieved by the enhancement of the strength of the rolled-up vortices in a way which will delay vortex breakdown. The enhancement of the strength of the concentrated vortex from the leading-edges of the slender wing can be achieved by generating a strong concentrated vortex, which will interact with the vortex system. Many devices have been proposed and used which generate vortices which interact with the main vortices from wing. These devices are modifications of the wing planform. The devices which were proposed for the generation of a strong vortex include the leading edge extensions (LEX), strakes and "saw tooth" modifications to the wing leading edges.

One useful method of enhancement of the delta wing performance is the use of a combination of multi-lifting surfaces such as using the vortex generated by the slender canard placed just ahead of and above, the main wing - the closed coupled wing-canard configuration. The closed coupled wing-canard configuration has the additional advantage of utilizing the canard as a movable aerodynamic control surface. In this case, the strength of the vortices generated by the movable canard can be increased by higher canard deflections. The close coupling between the canard and the wing will cause an upwash on the canard because of the wing

and a downwash on the wing because of the canard. These induced flows will affect the lift forces and moments on each one of these surfaces and, therefore, on the total lift force and the trim control effectiveness of the wing-canard configuration. wing-canard configuration are being used in a number of modern fighter aircraft such as the Swedish Draken J-35 and the new Gripen JAS-39, the proposed European Fighter Aircraft(EFA), the Israeli Kfir C-2 and the Lavi, the French Rafale as well in some versions proposed for the USAF Advanced Tactical Fighter (ATF).

As noted by Gloss and Washburn(1978) : " The proper use of canard surfaces on a maneuvering aircraft can offer several attractive features such as potentially higher trimmed- lift capability, improved pitching moment characteristics, and reduced trimmed drag. In addition, the geometrical characteristics of close-couple canard configurations offer a potential for improved longitudinal progression of cross-sectional area which could result in reduced wave drag at low supersonic speeds and placement of the horizontal control surfaces put of the high wing downwash and jet exhaust. These benefits are primarily associated with additional lift developed by the canard and with the beneficial interaction between the canard flow-field and that of the wing. These benefits may accompanied by a longitudinal instability (or pitch up) at the higher angles of attack because of the vortex lift developed on the forward canards. "

Another method of improving the aerodynamic performance of slender wings is the addition of the LEX(leading edge extension) in front of the main delta wing. Such configuration is used in the F-18 aircraft and the proposed Light Combat Aircraft of India.

The vortex generated by adding a slender strake as an extension on the leading

edge of the delta wing is found to enhance the strength of the main wing leading edge vortex, so as to delay vortex breakdown and increase the high angle of attack performance of the configuration. The aerodynamic characteristics of such configurations, specified as double-delta or strake- delta wings, were measured by Brennenstuhl and Hummel(1982) and were calculated by Gordon(1990)

Generation of leading edge vortices can thus be controlled by variations in the planform shapes such as double-delta, canard-wing combinations, leading-edge-extensions (LEX),sawtooth leading-edges, and others. These configurations, which utilize the strong vortex interaction, gives the aerodynamic designer new tools for controlled flight at very high angles of attack required for sharp maneuvers. Furthermore, introduction of small fins, acting as vortex generators at strategic positions, controlled by suitable control systems,can affect the complete flow field because of the interaction of the generated vortex filament from the fin with the vortex structure established on the configuration before the addition of the fin. Therefore, it may be said that properly controlled vortex interactions may enable significant variation of the overall lift on the aircraft with or without change of its attitude. Thus, controlled vortex interactions can be used as form of direct lift control.

1.4 Scope of the Present Work

The delta wings have an important role to play in the design on combat aircraft and missiles where high angles of attack are expected. A lot of experimental work has been done as enumerated above and delta wings and related more beneficial configurations have been used in aircraft design. There is increasing interest in the computational analysis due to the flexibility of testing of various configurations.

A lot of computational work has also been carried out a large part of which has been restricted to potential solutions. Euler solutions also have been used with success for such flow fields. Navier-Stokes solutions have a brief history of about a decade or so and current interest in high angles of attack aerodynamics is largely in this direction. The present work encompasses incompressible flow solution for flow about a sharp edged delta wing by Marker-and-Cell (MAC) algorithm for the main characteristics of the flow field. An attempt has been made to study the flow field associated with delta wings.

Chapter 2

Review of Literature

The importance and current interest in the delta wing configuration for aircraft design is discussed in the previous chapter. It is not recently that researchers have started to take interest in this field but a lot of work analytical, experimental, and computational has been done in the past. This chapter is an account of the attempts at understanding, analysis, and explanations of the flow field about delta wings and some closely related forms. Main theories that have been put forward are briefly outlined. Some of the theories and models proposed to explain and analyse the flow are listed below.

The earliest studies on the flows on delta wings were experimental. The experimentally observed rolling-up of vortices above the leading edges of slender delta wings led to investigation of simplified analytical and computational models of such flows. Considering the question of the aerodynamic properties of wings of large chord relative to their span (small AR), Betz (1933) proposed that the aerodynamic force on such a wing is due to mainly the drag force which is caused by the normal component of the velocity in the cross-plane. This model is referred to as *Cross Flow Model*. Interestingly enough, this extremely simplified analysis gave a

reasonable first order estimation for the non-linear lift of small AR wings.

Leading-Edge Vortex Models for Slender Delta Wings utilized the linearized conical flow models for slender delta wings of R. T. Jones(1946) and the concept of Legendre(1952) to add concentrated line vortices into the flow above the wing. Brown and Michael(1955) have used a procedure where the rolled up spiral sheet is replaced by a concentrated vortex near the spiral center. For conical flow, the net vorticity in the free vortex linearly increases in the flow direction ; therefore, the strength of the concentrated vortex must also increase in the streamwise direction. This increase in the strength was accomplished by assuming a plane feeding vortex sheet, an assumption satisfying Kelvin's theorem, between the leading edge and the vortex core.

The method of Brown and Michael(1955) was improved by allowing the vortex sheet, separating from the leading-edge of the delta wing to form the shape of a spiral vortex sheet. This method, *Spiral Vortex Sheet Model*, was proposed by Mangler and Smith (1959). The experimental measurements of the lift coefficients of delta wings of various AR showed that the conical parameters did not correlate well with the experimental data. The results of Brown and Michael (1955) were too high but those of Mangler and Smith were well within the range implying improvement due to spiral sheet model.

In *Leading Edge Suction Analogy* , developed by Polhamus(1966), the potential flow is modified to include the effects of high angles of attack and leading edge conditions. The vortex lift is assumed to be related to the potential flow about the leading edge. The vortex lift is evaluated utilizing the leading-edge flow model proposed by Polhamus(1966), where the force required to maintain the equilibrium of

the flow over the separated spiral leading edge vortex (provided that the flow reattaches at the upper surface) is equated with the force associated with the theoretical leading-edge singularity for thin wings in potential flow.

The concept that three-dimensional separation flows evolving from free rolled-up vortices can be modelled by an essentially inviscid potential flow field by introducing vortices along specified boundaries (thus confining the vortical flow to limited regions in the essentially inviscid flow field) has been the basis of the various linear and nonlinear potential panel methods discussed below. Panel methods have been used for flow calculations before computational power was in too limited to handle Euler or Navier-Stokes equations. Panel methods can provide fast and preliminary results for the purpose of design. In panel methods distribution of singularities, sources and doublets or vortices on the surface in question is used to calculate the aerodynamic characteristics.

The theoretical method of Multhopp (1950) has received wide acceptance as an accurate method for calculating aerodynamic load distributions on wings of various shapes in low speed flows. The method was modified and formulated for complex planform shapes, which are used in modern high performance aircraft, and adopted into a form suitable for programming for high speed digital computers by Lamar(1968).

The potential equation, the Laplace equation, can be solved under very general conditions by superposition of elementary solutions. A method based on distribution of sources over the surfaces of the configuration was developed at the Douglas Aircraft Company, and a general review of this method *The Surface-Source Method* is presented by Hess and Smith (1966) and Smith(1975).

In linear panel methods the trailing vortices from all the the panels are required to remain attached to the lifting surface; it is also assumed that these trailing vortices are separated only from the trailing edge and constitute a wake whose shape is flat sheet in the lane of the wing. In order to simulate the flow field in the nonlinear case, the panel methods must be modified. The free vortices must be allowed to separate from the lifting surfaces. In addition to the vortex separation from the trailing edge, it is usual to allow for vortex separaton from leading- and side edges and from separation lines on body surfaces. These methods can be also modified to include in their calculations the determination of the shape and position of the free rolled-up vortex lines or vortex sheets. Generally, such calculations must involve certain iteration procedures.

The solution of the Euler Equations has the advantage over the potential equation solution solution of providing the correct Rankine-Hugoniot shock wave jump conditions. Furthermore, the Euler equations are able to capture regions of vortical flows generated at certain parts of the aerodynamic configuration. The generation of vorticity in the inviscid flow can be explained by applying Crocco's theorem which equates the vorticity to the gradients of entropy in inviscid steady flow. Therefore, it is reasonable to assume that the complete flow field, except for isolated zones of vortex generation, can be calculated by the solution of inviscid Euler equations. The flow over a 55 deg cropped-delta wing was calculated by Eriksson and Rizzi(1984) using the time marching finite volume method to obtain steady state solution to the Euler equations. The leading edge vortex was captured and the roll-up of the leading edge vortex was clearly obtained.

Various Finite Volume Methods have been used for Euler solution. The method

presented by Jameson, Schmidt and Turkel(1981) has been modified by many workers. For example, Agarwal and Deese(1983), Volpe, Siclari and Jameson (1987a, 1987b). Another finite volume method was developed by Rizzi and Eriksson(1981,1984, 1985), Rizzi(1982) and Eriksson(1982). Rizzi and Eriksson proposed a method to solve Euler equations in their integral form by a pseudo-unsteady approach that marches a hyperbolic system of equations forward in time, without strict concern for time accuracy until a steady state is reached.

Euler equations have been solved by finite element method by Peraire et al. (1987), Angrand et al. (1985).

Raj et al. presented calculations of the aerodynamic characteristics of a sharp edged cropped delta wing. The computational method was based on the explicit finite volume, multistage Runge-Kutta psuedo-time-stepping algorithm for the solution of the three-dimensional Euler equations, designed as the TEAM code. The calculation initiated with the entire domain is at free stream conditions. Although no Kutta condition is explicitly applied, the leading-edge vortices are simulated.

Navier-Stokes equations represent the conservation laws of momentum, mass, and energy for fluid flow. Therefore, they are expected to simulate all the subtleties of fluid flow correctly provided the boundary conditions are imposed and in effect the problem is well posed. It is expected that the Navier-Stokes equations are capable of capturing the vortical flow structures such as the rolled up vortices and the three-dimensional vortex sheets generated in the flows over delta wings and related configurations. Hsu and Liu (1992) have presented results for three-dimensional viscous flow past a double-delta wing and a delta wing using an implicit upwind-relaxation finite-difference algorithm with a nonsingular eigensystem

to solve the preconditioned , three-dimensional, incompressible Navier-Stokes equations in curvilinear coordinates. An algebraic turbulence model was implemented. Hsu and Liu (1990) computed vortical flows over a thin round-edged double-delta wing using an implicit upwind-relaxation finite-difference scheme. Thomas, Krist and Anderson (1990) have presented results for Navier-Stokes computations using finite-volume algorithm. Thomas and Newsome (1989) performed Navier-Stokes computations flows over delta wings usigng an implicit algorithm employing upwind differencing for the pressure and convection terms and central differencing for the shear terms. Agrawal et. al. (1992) performed numerical investigation of leading-edge vortex breakdown on a flat-plate delta wing with sharp leading edges. They used both Euler and Navier-Stokes equations and reported that N-S equations showed significant improvement in breakdown location at high angles attack where the breakdown location approaches the apex.

Chapter 3

Mathematical Formulation

3.1 Introduction

There is currently a lot of interest in the high angle of attack aerodynamics as discussed in the previous chapters. Preliminary ideas regarding the flow field around configurations can be obtained by computational analysis of the relevant mathematical models. This has the advantage of providing data which can be used to design experiments for the detailed design. With improved models and solution techniques this can be taken to a situation where the full configurations with all the complexities can be analysed. This is what is being aimed at by the researchers active in this field. Present work, however, is a modest attempt at studying the features of flow about a sharp edged delta wing.

3.2 Statement of the Problem

3.2.1 Governing Equations

Computation is performed for incompressible flow about a sharp edged delta wing. Flow field is simulated by the Navier-Stokes equations which represent mass and

momentum conservation for fluids. The Navier-Stokes equations are capable of describing almost all fluid flow phenomena. Full Navier-Stokes equations are solved for the present problem.

Navier-Stokes equations for incompressible laminar flow in dimensionless form in Cartesian coordinates are written as

$$\frac{\partial U}{\partial X} + \frac{\partial V}{\partial Y} + \frac{\partial W}{\partial Z} = 0 \quad (3.1)$$

$$\frac{\partial U}{\partial t} + \frac{\partial U^2}{\partial X} + \frac{\partial UV}{\partial Y} + \frac{\partial UW}{\partial Z} = -\frac{\partial P}{\partial X} + \frac{1}{Re} \left[\frac{\partial^2 U}{\partial X^2} + \frac{\partial^2 U}{\partial Y^2} + \frac{\partial^2 U}{\partial Z^2} \right] \quad (3.2)$$

$$\frac{\partial V}{\partial t} + \frac{\partial VU}{\partial X} + \frac{\partial V^2}{\partial Y} + \frac{\partial VW}{\partial Z} = -\frac{\partial P}{\partial Y} + \frac{1}{Re} \left[\frac{\partial^2 V}{\partial X^2} + \frac{\partial^2 V}{\partial Y^2} + \frac{\partial^2 V}{\partial Z^2} \right] \quad (3.3)$$

$$\frac{\partial W}{\partial t} + \frac{\partial UW}{\partial X} + \frac{\partial VW}{\partial Y} + \frac{\partial W^2}{\partial Z} = -\frac{\partial P}{\partial Z} + \frac{1}{Re} \left[\frac{\partial^2 W}{\partial X^2} + \frac{\partial^2 W}{\partial Y^2} + \frac{\partial^2 W}{\partial Z^2} \right] \quad (3.4)$$

In the above equations the velocities have been nondimensionalized with the free stream velocity U_∞ and all lengths with the root chord of the wing, C_r . The pressure with ρU_∞^2 . No assumptions regarding the relative magnitudes of the different terms have been made in this study.

3.2.2 Grid

For the computational work a grid is generated which divides the domain of interest into a number of cells. The choice of grid system is dependent on the kinds of geometry involved in the computation. The grid used in the present case is a simple Cartesian grid which is formed by taking planes parallel to the three axes. The computational domain is divided into a number of rectangular cells of edge length δX , δY and δZ along the X, Y and Z directions respectively (fig. 3.1). Cells are denoted by an index (i,j,k) implying the cell number as counted from the origin in X, Y and Z directions respectively. Staggered grid arrangement is used (fig. 3.2).

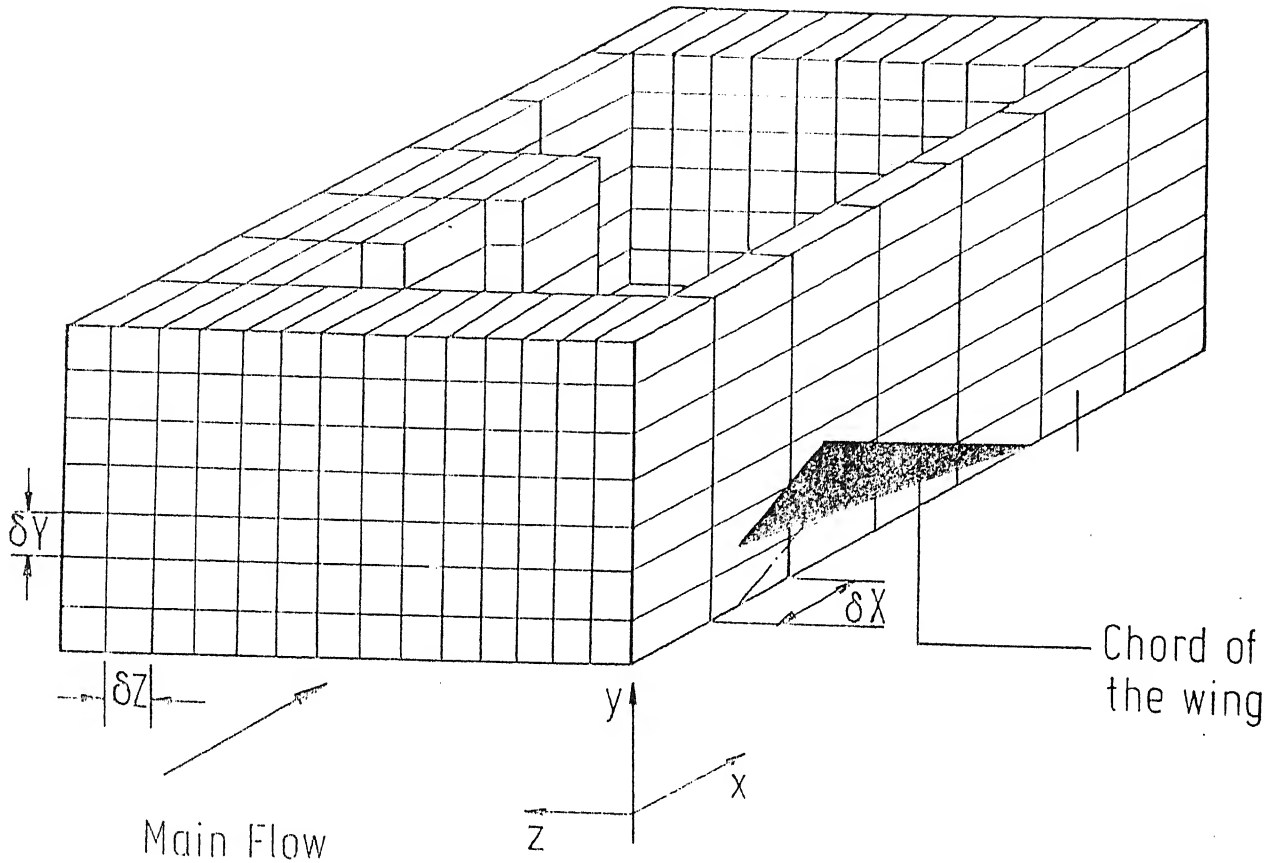


Figure 3.1: Grid spacing in the computational domain

The velocities are defined at the centers of the cell-faces to which they are normal. The relative positioning of the velocities and the wing surface in the XY plane is shown in fig. 3.3. The pressure is defined at the center of the cell (fig. 3.2).

3.2.3 Boundary Conditions

Proper boundary conditions have to be prescribed accurately for the correct description of the flow under study. Imposition of correct boundary conditions is even more important when the equations are discretized where the truncation errors

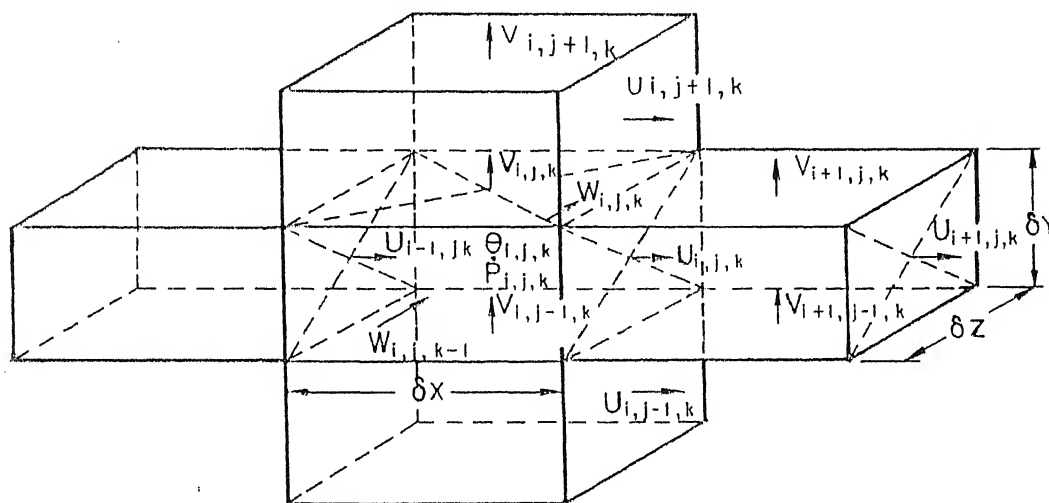


Figure 3.2: Three dimensional staggered grid with relative location of the variables

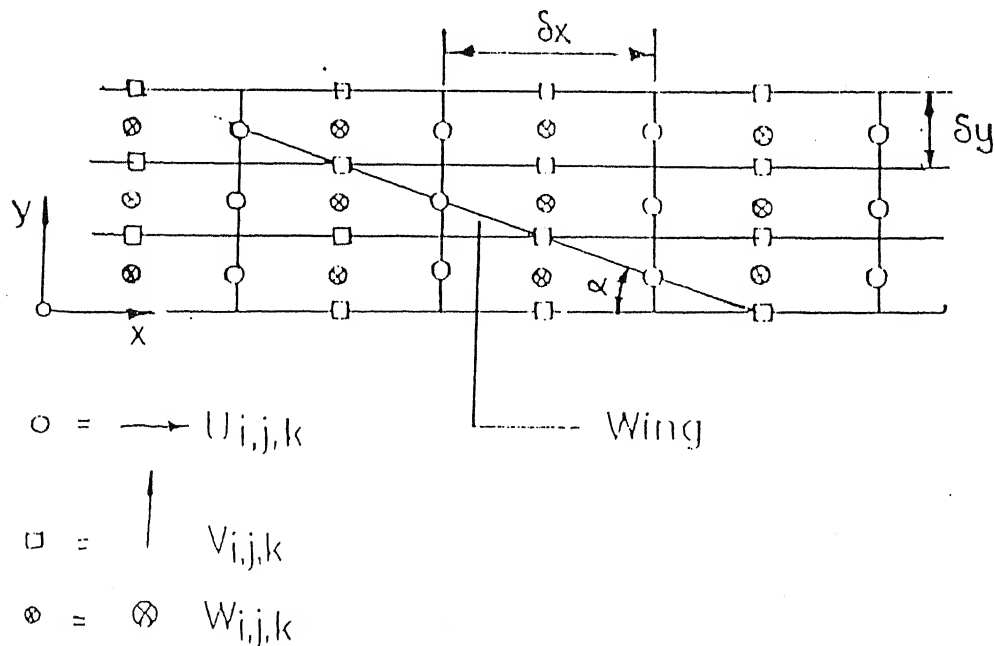


Figure 3.3: Relative location of the velocities and the wing surface (XY plane)

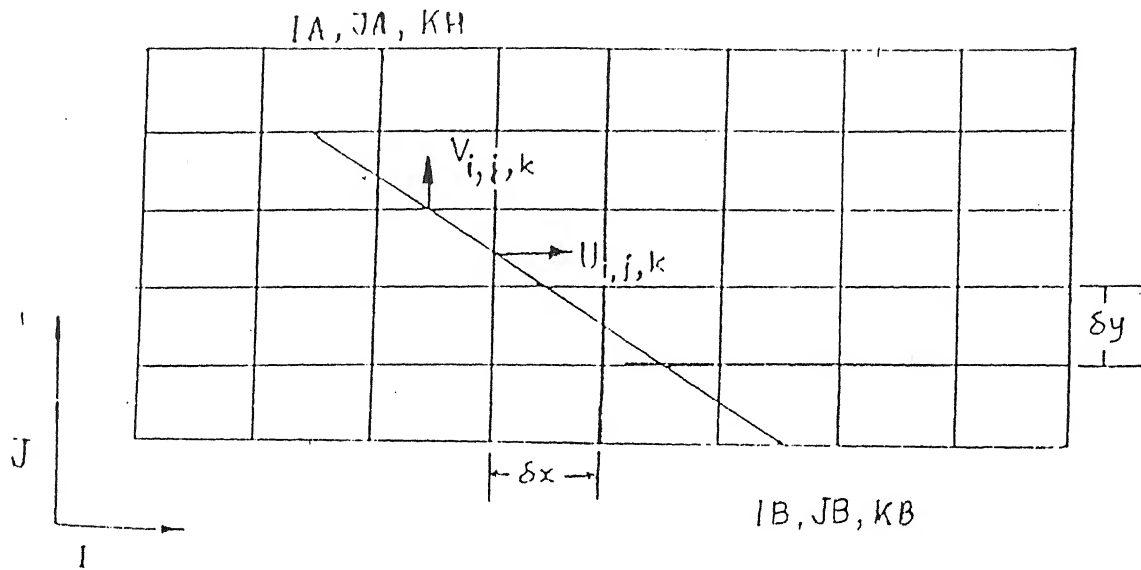


Figure 3.4: Velocity boundary conditions on the wing

creep in. Boundary conditions for this flow situation are

- On the wing surface:

All the velocity components directly falling on the wing surface are put to zero (fig. 3.4). Implementation of no-slip condition for U-component needs some manipulations. From fig. 3.5 it can be seen that $U_{i,j,k+\frac{1}{2}} = 0$. In the program it is implemented as

$$U_{i,j,k} = U_{i,j,k+1} \quad (3.5)$$

for $i=ia$ to ib , $j=jb$ to ja and $k=kh-(i-ia)$ to $kh+(i-ia)$. The W-components of velocity which also are not located on the wing are treated similarly (fig. 3.6)

- confining boundaries of the domain :

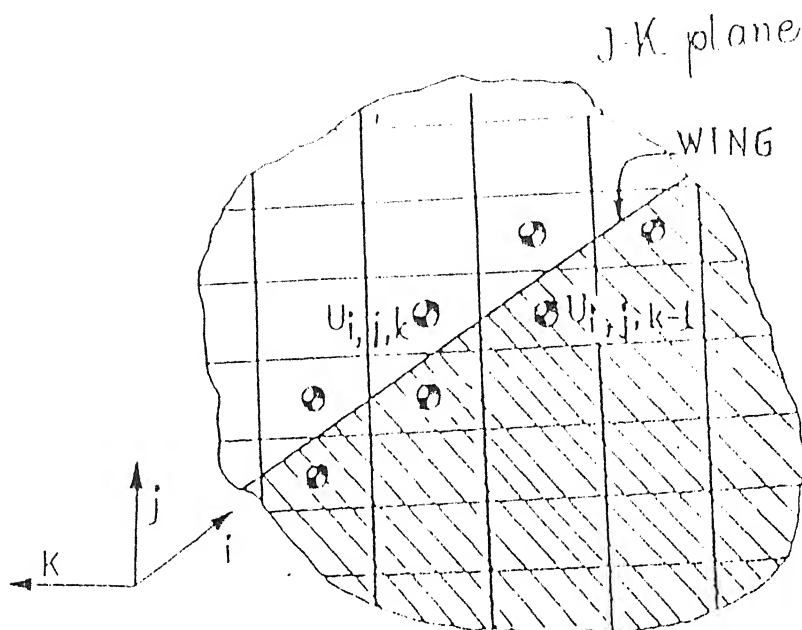


Figure 3.5: U-components on the wing surface

The normal velocity components are put to zero and the first derivative of the tangential components are put to zero (the velocities just outside the computational domain are put equal to those just inside).

$$\begin{aligned}
 U_{i,j,k} &= U_{i,j,k-1}, & V_{i,j,k} &= V_{i,j,k-1}, & W_{i,j,k} &= 0 & \forall i, j \text{ and } k = k_{im} \\
 U_{i,j,k} &= U_{i,j,k+1}, & V_{i,j,k} &= V_{i,j,k+1}, & W_{i,j,k} &= 0 & \forall i, j \text{ and } k = 2 \\
 U_{i,j,k} &= U_{i,j-1,k}, & W_{i,j,k} &= W_{i,j-1,k}, & V_{i,j,k} &= 0 & \forall i, k \text{ and } j = j_{im} \\
 U_{i,j,k} &= U_{i,j+1,k}, & W_{i,j,k} &= W_{i,j+1,k}, & V_{i,j,k} &= 0 & \forall i, k \text{ and } j = 2
 \end{aligned}$$

- inflow :

The normal component of velocity, U , is put to desired value and the tangential components, V and W , are put to zero.

$$U_{i,j,k} = 1.0 \quad V_{i,j,k} = 0 \quad W_{i,j,k} = 0 \quad \forall j, k \text{ and } i = 1$$

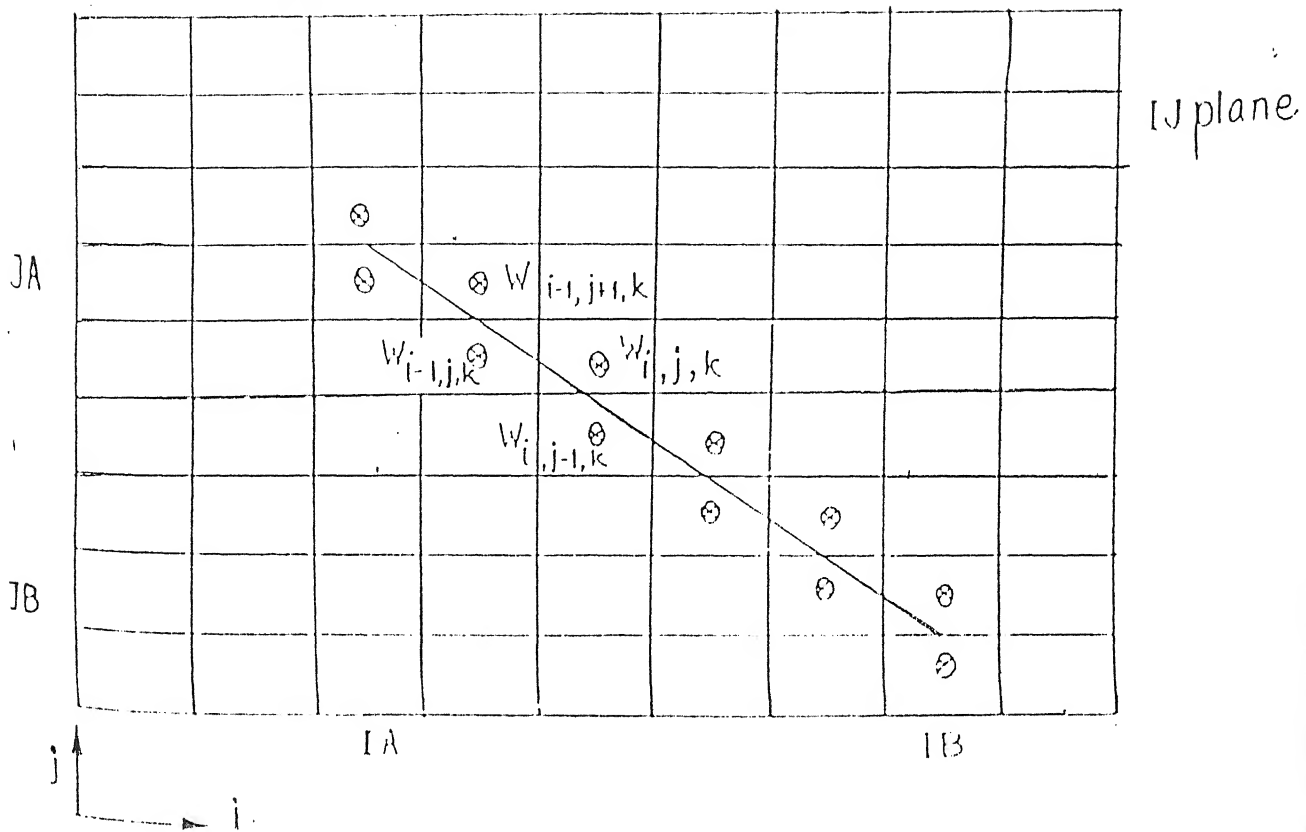


Figure 3.6: W-components on the wing surface

- outflow :

There is no unique prescription for outflow conditions. The idea is to have such conditions which do not affect the flow in the upstream. The second or higher order derivatives of all the velocity components in the streamwise direction are put to zero.

$$\frac{\partial^2 U}{\partial X^2} = \frac{\partial^2 V}{\partial Y^2} = \frac{\partial^2 W}{\partial Z^2} = 0$$

3.3 Discretization of the Equations

3.3.1 Continuity Equation

First order differencing is used for the discretization of the continuity equation. The discretized mass continuity equation is written as:

$$\begin{aligned} & (U_{i,j,k} - U_{i-1,j,k})/\delta X \\ & + (V_{i,j,k} - V_{i,j-1,k})/\delta Y \\ & + (W_{i,j,k} - W_{i,j,k-1})/\delta Z = 0 \end{aligned} \quad (3.6)$$

3.3.2 Momentum Equations

The convective terms of the momentum equations are discretized by a hybrid scheme which combines first order upwind and central differencing to achieve the stability of upwind and formal accuracy of the central differencing (Spalding (1972)). The discretization of one of the convective terms is shown below:

$$\begin{aligned} \frac{\partial(UV)}{\partial Y} = & \frac{1}{4\delta Y} [(V_{i,j,k} + V_{i+1,j,k})(U_{i,j,k} + U_{i,j+1,k}) \\ & + \alpha |(V_{i,j,k} + V_{i+1,j,k})|(U_{i,j,k} - U_{i,j+1,k}) \\ & - (V_{i,j-1,k} + V_{i+1,j-1,k})(U_{i,j-1,k} + U_{i,j,k}) \\ & - \alpha |(V_{i,j-1,k} - V_{i+1,j-1,k})|(U_{i,j-1,k} - U_{i,j,k})] \end{aligned} \quad (3.7)$$

and similar terms for the Y- and Z- components of the momentum equations. The factor α determines the relative weightage of the central and upwind differencing. $\alpha = 0$ gives simple central differencing and $\alpha = 1$ gives second upwind differencing. The value of this factor is determined by the stability criteria.

Temporal derivatives are discretized by simple forward differencing:

$$\frac{\partial U}{\partial t} = (U_{i,j,k}^{n+1} - U_{i,j,k}^n) / \delta t \quad (3.8)$$

Diffusion terms are discretized using second order differencing

$$\frac{\partial^2 U}{\partial X^2} = \frac{1}{(\delta X)^2} [U_{i+1,j,k} - 2U_{i,j,k} + U_{i-1,j,k}] \quad (3.9)$$

3.4 Marker-and-Cell Method

The nondimensional continuity, momentum and energy equations in conservative forms, written in terms of primitive variables, are solved by using a modified version of Marker and Cell (MAC) algorithm. The original version of MAC due to Harlow and Welch (1965) was modified by Hirt and Cook (1972). In the original MAC method, the pressure field was obtained by directly solving the Poisson's equation for pressure, whereas, in modified MAC version, pressure values are calculated implicitly from continuity equation by a pressure-velocity iteration process. A related technique developed by Chorin (1967) involved a simultaneous iteration on pressure and velocity components. Vieceilli (1971) has shown that the two methods as applied to the MAC algorithm are equivalent.

3.4.1 Salient Features

The Marker and Cell method (MAC) method of Harlow & Welch (1965) is one of the earliest and most useful method for solving Navier-Stokes equations. This method necessarily deals with a Poisson equation for the pressure and momentum equation for velocities. The MAC method was developed to solve problems with free surfaces, but it can be applied to any incompressible fluid flow problems. A modified version

of Hirt & Cook (1972) has been used by many researchers to solve a variety of fluid flow problems.

Following are the salient features of the MAC method :

- Unsteady Navier-Stokes equations for incompressible flow with weak conservative form and the continuity equation are the governing equations.
- Description of the problem is elliptic in space and parabolic in time. Solution is therefore found by marching in time. At each step, converged solution in space domain is obtained but this converged solution at any time-step may not be the solution of the physical problem.
- If the problem is steady, in its physical sense, then after a finite number of steps in time direction, two consecutive time-steps will show the identical solutions. However, in a machine computation this is not possible hence a very small value STAT is predefined. Typically STAT may be chosen between 10^{-3} and 10^{-5} . If the maximum change in any of the velocity components for two time steps does not exceed STAT then it can be said that the steady solution has been obtained.
- If the physical problem is basically unsteady in nature, the aforesaid maximum change will never be less than STAT. However, in such a situation, a velocity component may be stored over a number of time steps and analysed.
- With the use of momentum equation provisional velocities are computed.

3.4.2 Computational Scheme

MAC is a semi-implicit scheme of solving complete unsteady Navier-Stokes equations where the advancement of velocity components with respect to time are obtained explicitly by calculating accelerations due to convection, diffusion and pressure gradient. After obtaining a provisional velocity field for a particular time-step, the continuity equation is solved implicitly. Hence MAC is an implicit-explicit scheme.

The complete Navier-Stokes equations are elliptic in space and parabolic in time. Hence their solution has to time-marching. Again, since the equations are elliptic in space, we need boundary conditions on all confining boundaries - even at the outlet. To start the computation, guess field of velocity and pressure is assumed.

From the guessed velocity and pressure fields, the corrected velocity and pressure fields are obtained by pressure-velocity iteration through continuity equation. Convergence of this iteration process ensures a divergence-free velocity field for the initial time-step. Now, this corrected pressure-velocity field is used to calculate the velocity field for the next time step by making use of Navier-Stokes equations. The advancement of the velocity for one time step δt is calculated by evaluating the accelerations caused by advection, diffusion and pressure gradient. The choice of the time increment value δt is governed by numerical stability criteria. However, this explicit time advancement may not lead to a velocity field with zero mass divergence in each cell. In the subsequent stage, adjustments are done to ensure mass conservation in each cell. This is performed by manipulating the pressure as well as velocities in each cell through an iterative process, which, as mentioned earlier is equivalent to solution of Poisson equation for pressure.

3.4.3 Pressure-Velocity Iteration

As there is no pressure boundary condition the solution of Poisson equation is accomplished in an iterative manner. In the original MAC method the Poisson equation was solved for pressure. The modification due to Hirt & Cook (1972) enables one to solve the Poisson equation in such a way that the velocity and pressure fields are correct and satisfy the governing equations and the velocity boundary conditions are satisfied.

The velocities are advanced explicitly from the momentum equation if the velocities and pressures are known at any time step by calculating the accelerations due to advection, diffusion and pressure gradients. But these values are not necessarily the ones to give a meaningful solution if there is any non-zero value of the divergence. Pressures are correct if they are accompanied by zero divergence. The pressures have to be corrected such that there is no accumulation or annihilation of mass anywhere in the domain. Corrections to pressures are applied in an iterative manner as described by Hirt & Cook (1972) which as mentioned earlier is equivalent to the solution of a Poisson equation for pressure.

The method of pressure-velocity correction iteration is as follows. The relationship between the explicitly advanced velocity components at $(n+1)^{th}$ time level and that at the previous n^{th} time level can be put as

$$\tilde{U}_{i,j,k}^{n+1} = U_{i,j,k}^n + \left(\frac{\delta t}{\delta X} \right) (P_{i,j,k}^n - P_{i+1,j,k}^n) + \delta t [RESIDU]_{i,j,k}^n \quad (3.10)$$

where $[RESIDU]_{i,j,k}^n$ is the value of

$$\left[-\frac{\partial U^2}{\partial X} - \frac{\partial UV}{\partial Y} - \frac{\partial UW}{\partial Z} + \frac{\nabla^2 U}{Re} \right] \quad (3.11)$$

at the (i, j, k) cell evaluated with the velocity values at the n^{th} time step.

On the other hand, the corrected velocity components, which are still unknown, are related to the correct pressure (unknown) in the manner

$$U_{i,j,k}^{n+1} = U_{i,j,k}^n + \left(\frac{\delta t}{\delta X} \right) (P_{i,j,k}^{n+1} - P_{i+1,j,k}^{n+1}) + \delta t [RESIDU]_{i,j,k}^n \quad (3.12)$$

from equations 1.10 and 1.12 one can write

$$U_{i,j,k}^{n+1} - \tilde{U}_{i,j,k}^{n+1} = \left(\frac{\delta t}{\delta X} \right) (P'_{i,j,k} - P'_{i+1,j,k}) \quad (3.13)$$

where $P'_{i,j,k} = P_{i,j,k}^{n+1} - P_{i,j,k}^n$

Neither $\delta P'_{i,j,k}$ nor $U_{i,j,k}^{n+1}$ are explicitly known at this stage so that one can be calculated with the help of the other. Calculations are done in an iterative cycle and we can write

$$U_{i,j,k}^{n+1} \longrightarrow \tilde{U}_{i,j,k}^{n+1} + \left(\frac{\delta t}{\delta X} \right) (P_{i,j,k} - P'_{i+1,j,k}) \quad (3.14)$$

In the similar manner the other velocities can be written as

$$U_{i-1,j,k}^{n+1} \longrightarrow \tilde{U}_{i,j,k}^{n+1} - \left(\frac{\delta t}{\delta X} \right) (P'_{i,j,k} - P'_{i-1,j,k}) \quad (3.15)$$

$$V_{i,j,k}^{n+1} \longrightarrow \tilde{V}_{i,j,k}^{n+1} + \left(\frac{\delta t}{\delta Y} \right) (P'_{i,j,k} - P'_{i,j+1,k}) \quad (3.16)$$

$$V_{i,j-1,k}^{n+1} \longrightarrow \tilde{V}_{i,j,k}^{n+1} - \left(\frac{\delta t}{\delta Y} \right) (P'_{i,j,k} - P'_{i,j-1,k}) \quad (3.17)$$

$$W_{i,j,k+1}^{n+1} \longrightarrow \tilde{W}_{i,j,k}^{n+1} + \left(\frac{\delta t}{\delta Z} \right) (P'_{i,j,k} - P'_{i,j,k+1}) \quad (3.18)$$

$$W_{i,j,k-1}^{n+1} \longrightarrow \tilde{W}_{i,j,k}^{n+1} - \left(\frac{\delta t}{\delta Z} \right) (P'_{i,j,k} - P'_{i,j,k-1}) \quad (3.19)$$

The correction is done through continuity equation. Plugging in the relationships 3.14 to 3.19 into the continuity equation (3.6) we get,

$$\left[\frac{U_{i,j,k}^{n+1} - U_{i-1,j,k}^{n+1}}{\delta X} + \frac{V_{i,j,k}^{n+1} - V_{i,j-1,k}^{n+1}}{\delta Y} + \frac{W_{i,j,k}^{n+1} - W_{i,j,k-1}^{n+1}}{\delta Z} \right]$$

$$\begin{aligned}
&= \left[\frac{\tilde{U}_{i,j,k}^{n+1} - \tilde{U}_{i-1,j,k}^{n+1}}{\delta X} + \frac{\tilde{V}_{i,j,k}^{n+1} - \tilde{V}_{i,j-1,k}^{n+1}}{\delta Y} + \frac{\tilde{W}_{i,j,k}^{n+1} - \tilde{W}_{i,j,k-1}^{n+1}}{\delta Z} \right] \\
&\quad - \delta t \left[\frac{P'_{i+1,j,k} - 2P'_{i,j,k} + P'_{i-1,j,k}}{\delta X^2} \right] \\
&\quad - \delta t \left[\frac{P'_{i,j+1,k} - 2P'_{i,j,k} + P'_{i,j-1,k}}{\delta Y^2} \right] \\
&\quad - \delta t \left[\frac{P'_{i,j,k+1} - 2P'_{i,j,k} + P'_{i,j,k-1}}{\delta Z^2} \right] \tag{3.20}
\end{aligned}$$

The pressure corrections in the neighbouring cells are neglected. Therefore, we get the velocity corrections, 3.14 to 3.19, in the form,

$$U_{i,j,k}^{n+1} \longrightarrow \tilde{U}_{i,j,k}^{n+1} + \left(\frac{\delta t}{\delta X} \right) (P'_{i,j,k}) \tag{3.21}$$

$$U_{i-1,j,k}^{n+1} \longrightarrow \tilde{U}_{i,j,k}^{n+1} - \left(\frac{\delta t}{\delta X} \right) (P'_{i,j,k}) \tag{3.22}$$

$$V_{i,j,k}^{n+1} \longrightarrow \tilde{V}_{i,j,k}^{n+1} + \left(\frac{\delta t}{\delta Y} \right) (P'_{i,j,k}) \tag{3.23}$$

$$V_{i,j-1,k}^{n+1} \longrightarrow \tilde{V}_{i,j,k}^{n+1} - \left(\frac{\delta t}{\delta Y} \right) (P'_{i,j,k}) \tag{3.24}$$

$$W_{i,j,k+1}^{n+1} \longrightarrow \tilde{W}_{i,j,k}^{n+1} + \left(\frac{\delta t}{\delta Z} \right) (P'_{i,j,k}) \tag{3.25}$$

$$W_{i,j,k-1}^{n+1} \longrightarrow \tilde{W}_{i,j,k}^{n+1} - \left(\frac{\delta t}{\delta Z} \right) (P'_{i,j,k}) \tag{3.26}$$

The continuity equation takes the following form after neglecting the pressures corrections in the neighbouring cells,

$$\begin{aligned}
&\left[\frac{U_{i,j,k}^{n+1} - U_{i-1,j,k}^{n+1}}{\delta X} + \frac{V_{i,j,k}^{n+1} - V_{i,j-1,k}^{n+1}}{\delta Y} + \frac{W_{i,j,k}^{n+1} - W_{i,j,k-1}^{n+1}}{\delta Z} \right] \\
&= \left[\frac{\tilde{U}_{i,j,k}^{n+1} - \tilde{U}_{i-1,j,k}^{n+1}}{\delta X} + \frac{\tilde{V}_{i,j,k}^{n+1} - \tilde{V}_{i,j-1,k}^{n+1}}{\delta Y} + \frac{\tilde{W}_{i,j,k}^{n+1} - \tilde{W}_{i,j,k-1}^{n+1}}{\delta Z} \right] \\
&\quad + 2 \left(\frac{\delta t}{\delta X^2} \right) (P'_{i,j,k}) + 2 \left(\frac{\delta t}{\delta Y^2} \right) (P'_{i,j,k}) + 2 \left(\frac{\delta t}{\delta Z^2} \right) (P'_{i,j,k}) \tag{3.27}
\end{aligned}$$

or,

$$0 = \Delta_{i,j,k} + P'_{i,j,k} \left[2\delta t \left[\frac{1}{\delta X^2} + \frac{1}{\delta Y^2} + \frac{1}{\delta Z^2} \right] \right] \quad (3.28)$$

or,

$$P'_{i,j,k} = \omega_0 (\Delta_{i,j,k}) / [2\delta t \left[\frac{1}{\delta X^2} + \frac{1}{\delta Y^2} + \frac{1}{\delta Z^2} \right]] \quad (3.29)$$

where ω_0 is an over relaxation factor which is introduced to accelerate the pressure correction process. Usually a value of 1.7 is used. After calculating $\delta P'_{i,j,k}$, velocities in each cell are corrected according to the equation set and pressure in each cell is adjusted as

$$P_{i,j,k}^{n+1} \longrightarrow P_{i,j,k}^n + P'_{i,j,k} \quad (3.30)$$

This process is continued until the velocity divergence in each cell vanishes. If the velocity boundary conditions are correct and a divergence-free converged velocity field is obtained, eventually correct pressures will be evolved in all the cells including the cells on the boundary. This feature of modified MAC method has been discussed in more details by Peyret and Taylor (1983). However, it was also shown by Brandt, Dendy and Ruppel (1980) that the aforesaid pressure-velocity iteration procedure is equivalent to solution of Poisson Equation for pressure.

3.4.4 Stability Criteria

For a given mesh the choice of the time step is determined through stability analysis which has to take care of two conditions. First, fluid should not allowed to cross

more than one cell in one time step . This restriction is derived from the Courant-Friedrichs-Lewy (CFL) condition given by

$$\delta t_1 < \min\left(\frac{\delta X}{|U|}, \frac{\delta Y}{|V|}, \frac{\delta Z}{|W|}\right) \quad (3.31)$$

where the minimum is with respect to every cell in the domain. Typically δt is chosen equal to one-third to two-third of the minimum cell transient time.

Second, when a nonzero value of kinematic viscosity is used, momentum must not diffuse more than approximately one cell in one cell in one time step. A linear stability analysis shows that the restrictions on grid Fourier number will yield

$$\delta t_2 < \frac{1}{2} / \left(\frac{1}{\delta X^2} + \frac{1}{\delta Y^2} + \frac{1}{\delta Z^2} \right) Re \quad (3.32)$$

Finally, the minimum of the two time-steps is chosen for the computation.

The term α in the discretization of convective terms of the equations , which is a weighting factor which gives the desired amount amount of upstream (donor cell) differencing. $\alpha = 0$ gives space-centred differencing and $\alpha = 1$ gives full upstream or donor cell form, which is stable provided the fluid is not permitted to cross more than one cell in one time-step. In general, α should be chosen slightly larger than the maximum value of

$$\left| \frac{U \delta t}{\delta X} \right| \text{ or } \left| \frac{V \delta t}{\delta Y} \right| \text{ or } \left| \frac{W \delta t}{\delta Z} \right| \quad (3.33)$$

occurring in the entire domain. In other words

$$1 > \alpha > \max \left[\left| \frac{U \delta t}{\delta X} \right|, \left| \frac{V \delta t}{\delta Y} \right|, \left| \frac{W \delta t}{\delta Z} \right| \right] \quad (3.34)$$

Chapter 4

Results and Discussions

4.1 Velocity vectors

Computations have been performed for a slender delta wing in infinite medium. Studies have been accomplished at different angles of attack for the delta wing. A grid of $(23 \times 28 \times 41)$ is used for the calculations. There is 5 points ahead of the wing, 10 on the wing in the streamwise direction. In the normal direction there are 10 points on the wing. In the spanwise direction the number of points vary from 1 (at the tip) to 20 (at the trailing edge).

For slender delta wings in an infinite medium leading edge vortices have a spiralling structure and they diverge slightly. Now, when we envision a wing moving in an infinite medium, the wake grows longer and basically becomes a swirling flow supported by trailing edge vortices. A typical flow situation for a sharp edged delta wing is shown in fig. 4.1. The primary vortices are generated at the apex of the wing and then propagate downstream. Going further downstream, the trailing edge vortices boost the primary vortex and create a strong swirling flow. A large portion of the lift of the wing is contributed by these spiralling vortices which produce extra suction on the upper surface of the wing. However, angle of attack has a significant

influence on the strength of the vortex motion. This is evident from comparison between the figures 4.1 to 4.5. Wing theory shows that the lift for a small aspect ratio wing is proportional to the angle of attack α . With the increase in α delta wings generate additional lift which is a nonlinear function of α until the lift collapses at stall. Stall occurs at the highest value of angle of attack for small AR delta wings. However, the strength of the vortices is directly proportional to the lift. The computed results show some qualitative enhancement in the vortical motion through the higher magnitude of the velocity vectors corresponding to secondary flow at the same axial location for different angles of attack. Reynolds number for the above mentioned cases is kept constant and the value employed is 0.9×10^6 .

4.2 Pressure Distribution

The pressure distribution obtained at four sections of the wing and another cross-stream position behind the wing. The nondimensional static pressure contours follow the same qualitative trend as those observed in the experimental results of Hummel (1978). The first cross-stream view in the fig. 4.6 is a location $0.3C_r$ from the leading edge of the wing. The subsequent cross-stream views are $0.5C_r$, $0.7C_r$ and $0.9C_r$ respectively. The last view corresponds to pressure distribution in the wake $0.3C_r$ behind the trailing edge. Figures 4.7 to 4.10 show the influence of angle of attack on the pressure distribution. With increasing angle of attack the pressure distribution on the suction side decreases. The ability of convecting vorticity is enhanced. In the range of angles of attack the leading edge vortices are held in place and no shedding has been observed. The enhanced suction due to increasing angle of attack contributes to increased C_L which is discussed in a subsequent section. In the range

of angles of attack vortex breakdown has not taken place and the 3D equivalent of the 2D stall could not be observed.

The capability of the predictive procedure in demonstrating the pressure coefficients (fig. 4.11) for a delta wing of AR 1 at low subsonic speed. Fig. 4.12 to 4.15 show the detailed surface pressure distribution for the same delta wing at different angles of attack (25, 30, 35 and 40 degrees). For 50 degrees angle of attack the computation started to show oscillations after some iterations in the time direction and instead of monotonically converged results the maximum discrepancy between the dependent variables for two consecutive time steps started oscillating. Perhaps vortex breakdown takes place at that condition. A similar trend was observed by Biswas (1993) who uses the same numerical method as ours. fig. 4.16 shows the flow pattern for this case.

4.3 Vorticity Contours

Development of streamwise vorticity is presented in figure 4.17 for a low Reynolds number flow. dotted lines indicate negative vorticity. Peak vorticity occurs in the vortex centres. In the downstream the leading edge vortices expand in size. In an attached flow situation the vorticity is advected by the axial velocity. On a delta wing the amount of vorticity rolled up depends on the pressure differential between the suction and pressure sides. Polhamus (1971) predicted the total lift on the delta wing by separating the normal force into the potential and vortex components. The potential lift term is based on the lifting surface theory taking into consideration Kutta condition at the trailing edge. The vortex lift is modelled by the suction force generated by the equivalent attached flow around the edge.

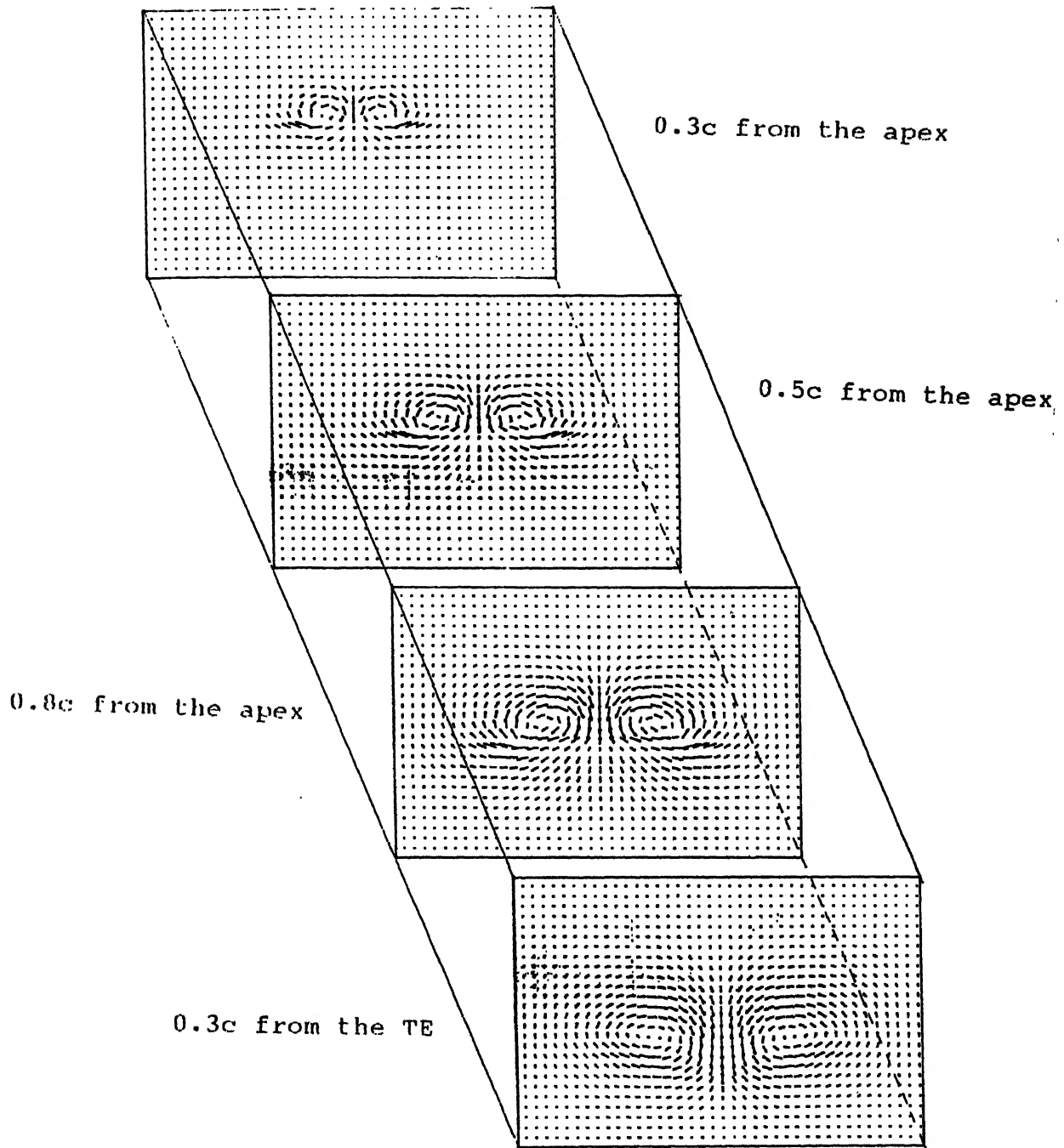


Figure 4.1: Cross-stream velocity vectors at different axial locations ($\alpha = 20.5$)

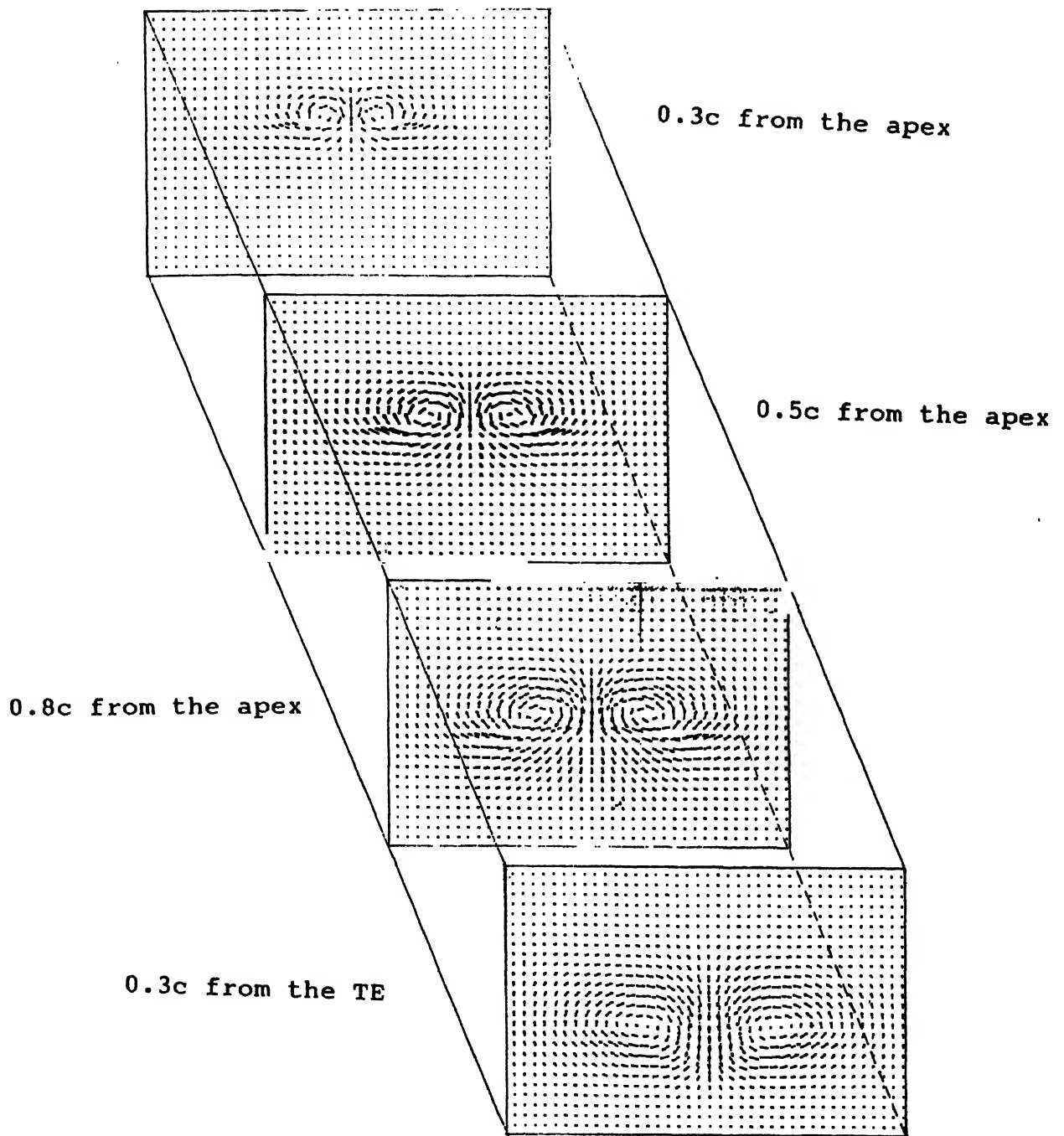


Figure 4.2: Cross-stream velocity vectors at different axial locations ($\alpha = 25$)

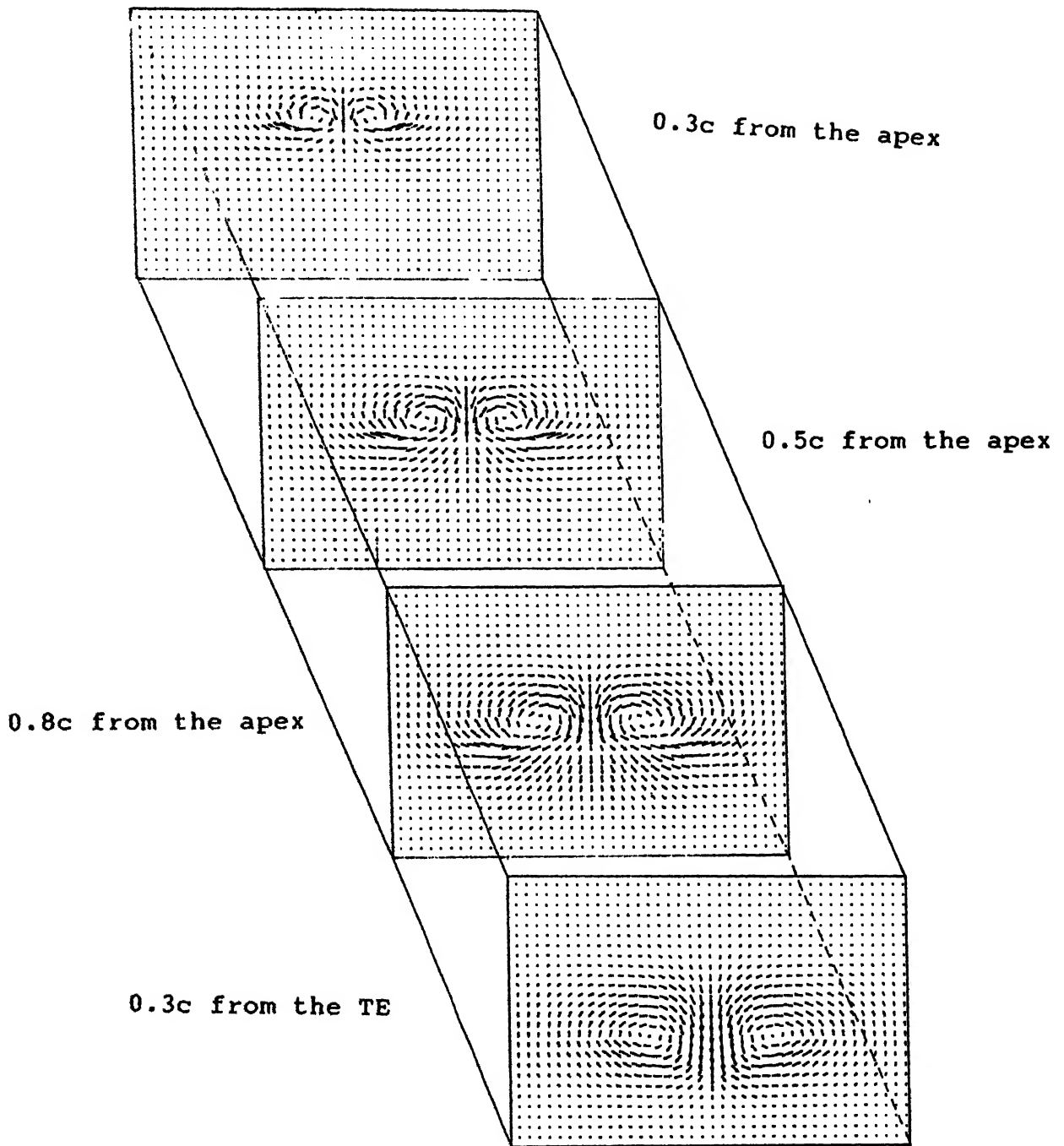


Figure 4.3: Cross-stream velocity vectors at different axial locations ($\alpha = 30$)

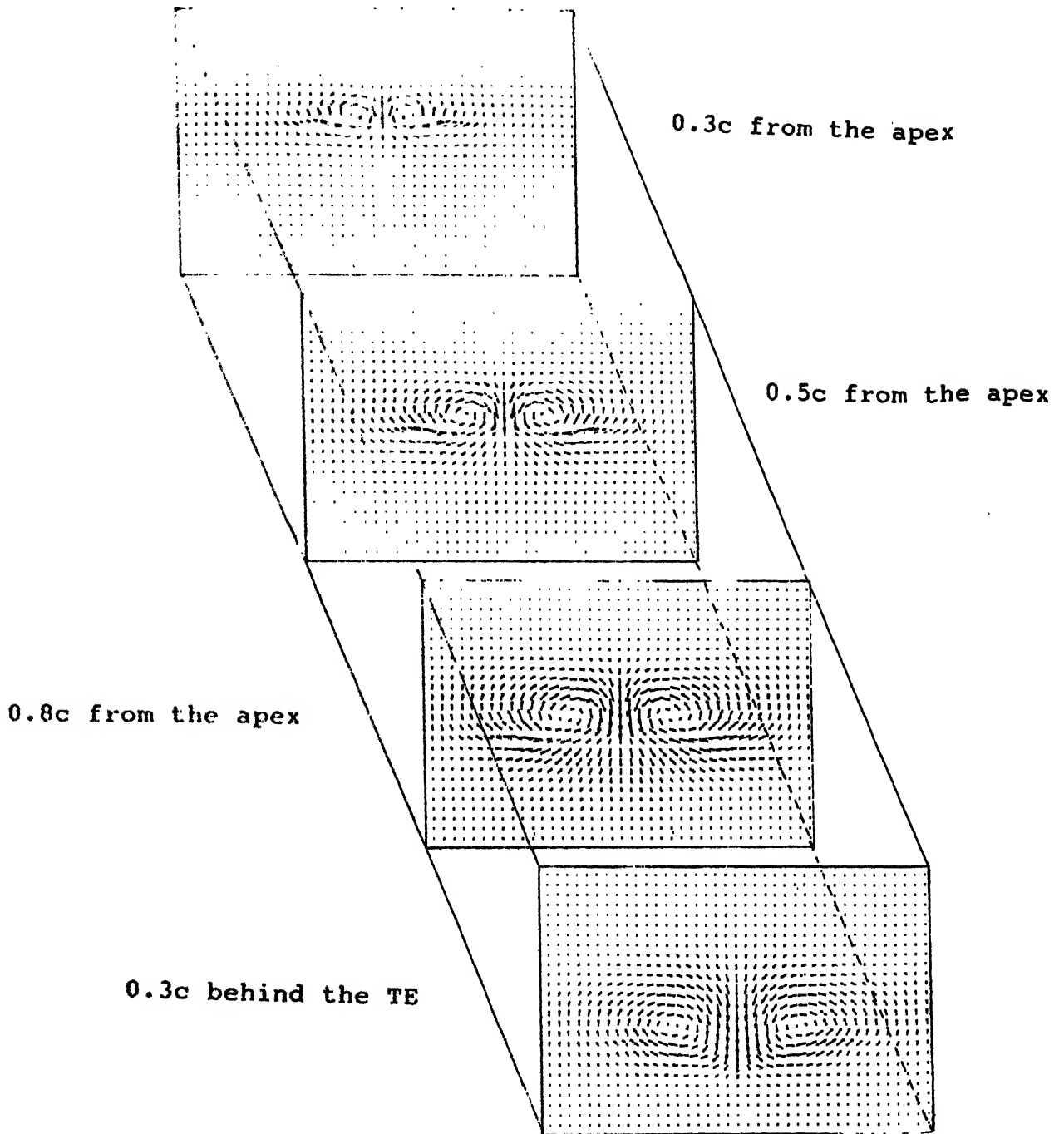


Figure 4.4: Cross-stream velocity vectors at different axial locations ($\alpha = 35$)

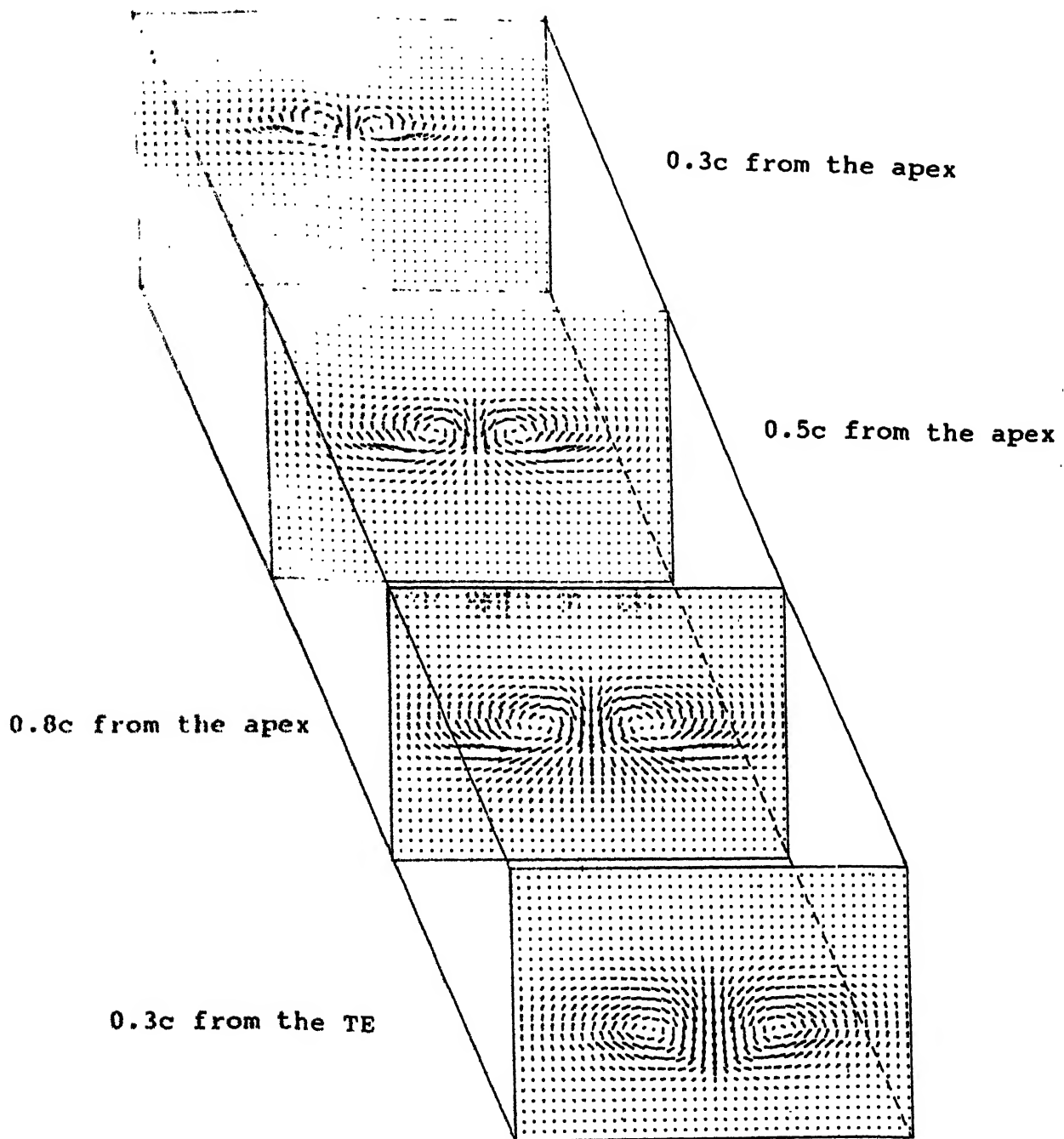


Figure 4.5: Cross-stream velocity vectors at different axial locations ($\alpha = 40$)

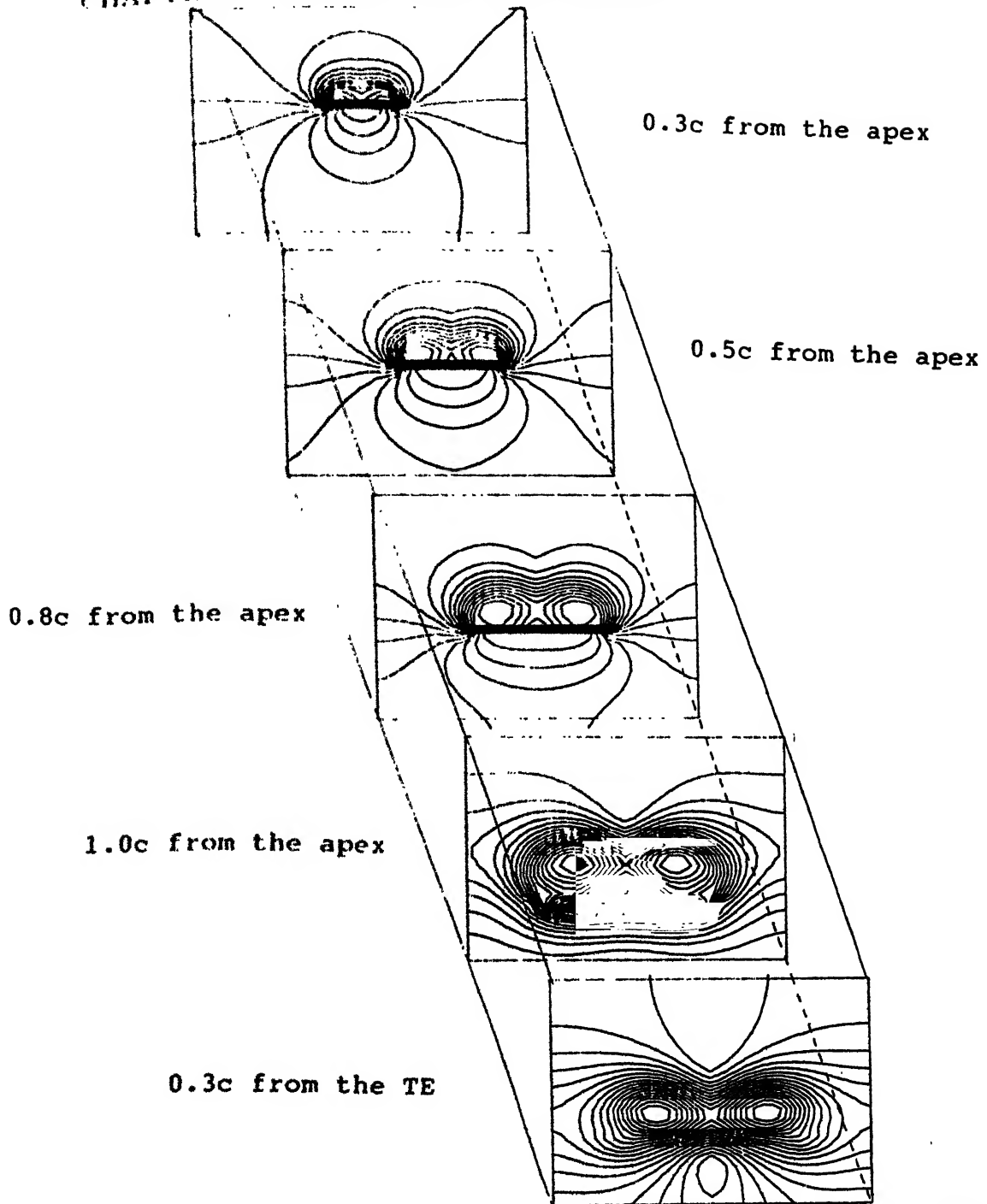


Figure 4.6: Pressure contours at different axial locations ($\alpha = 20.5$)

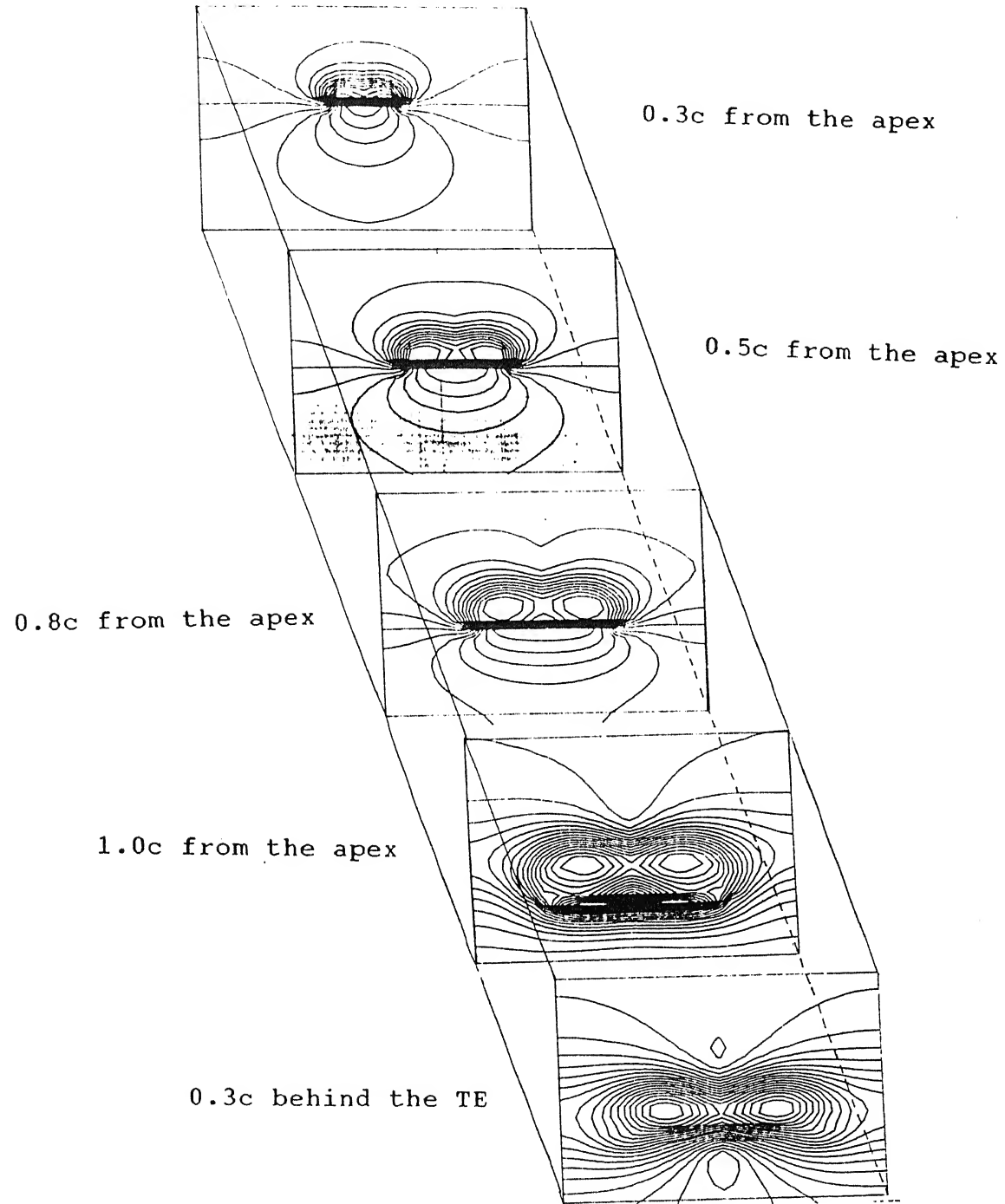


Figure 4.7: Pressure contours at different axial locations ($\alpha = 25$)

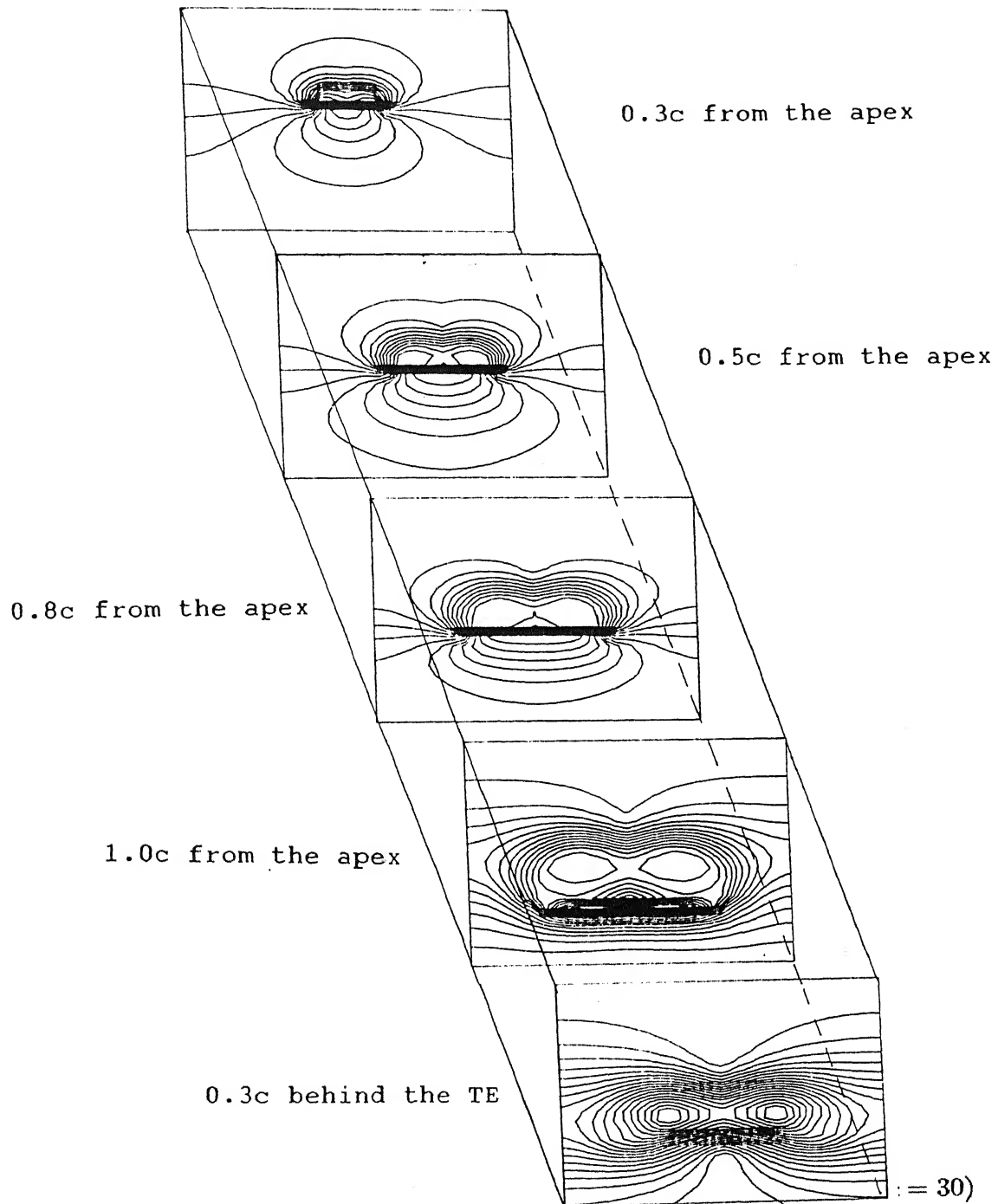


Figure 4.8: Pressure contours at different axial locations ($\alpha = 30^\circ$)

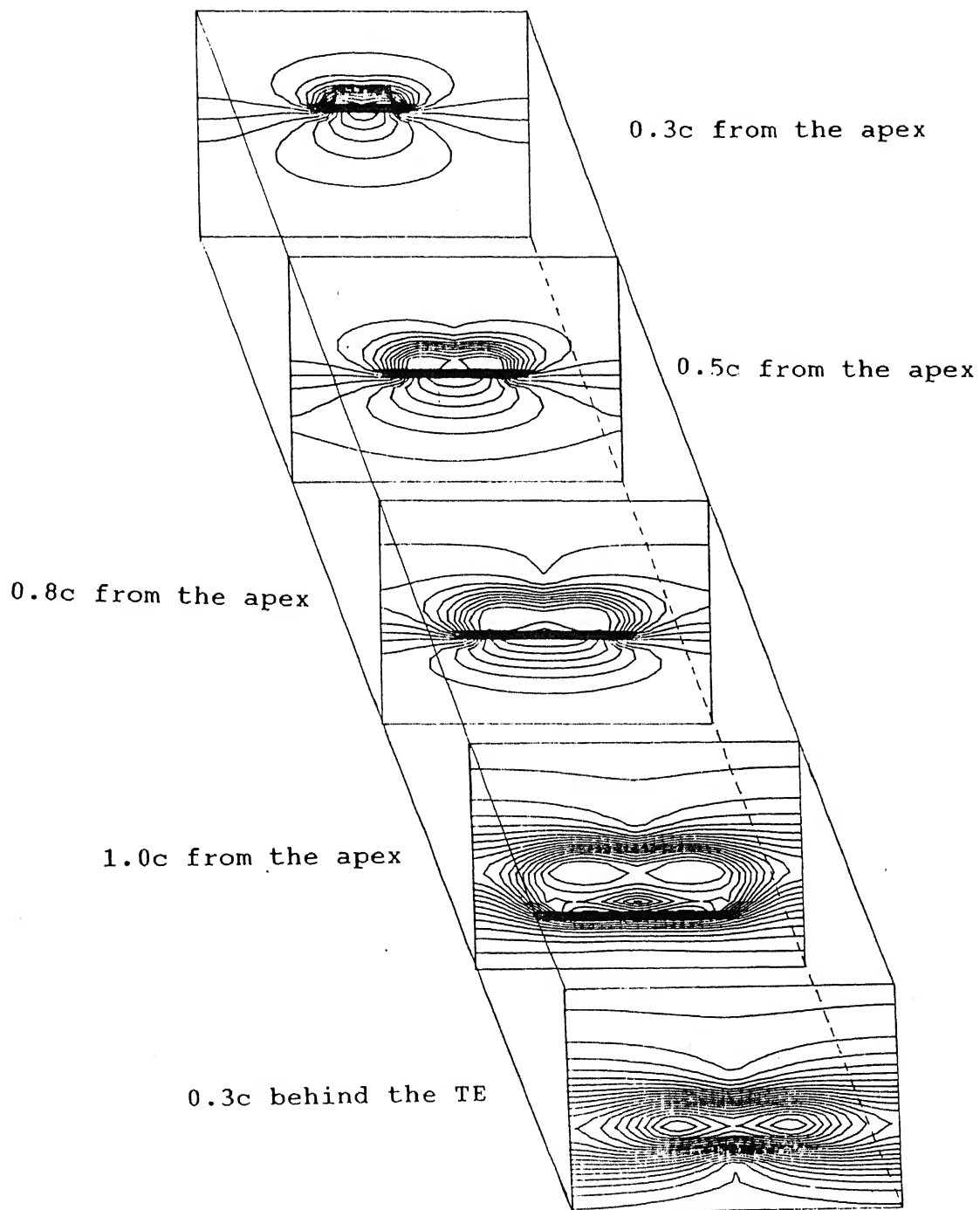


Figure 4.9: Pressure contours at different axial locations ($\alpha = 35$)

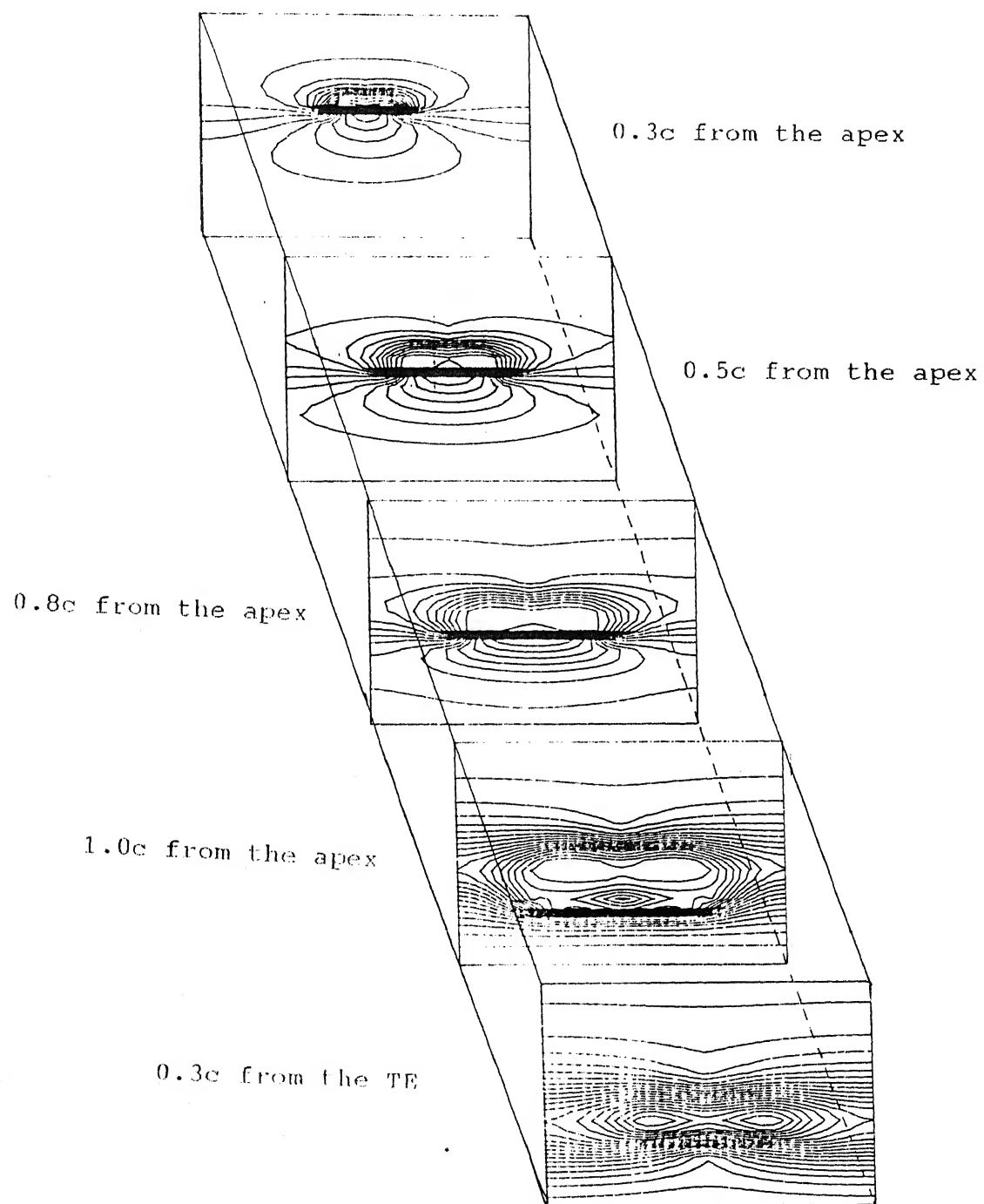
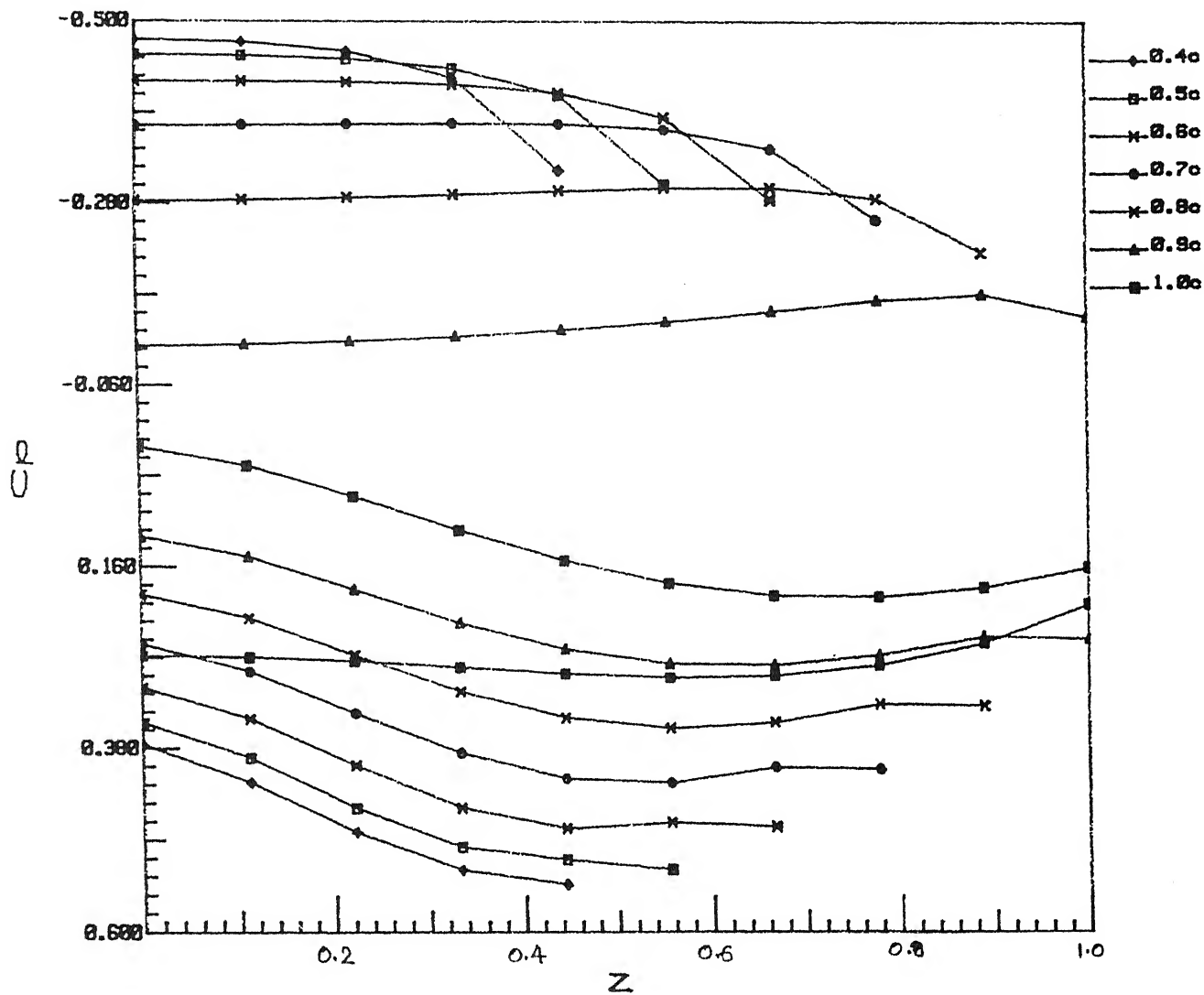
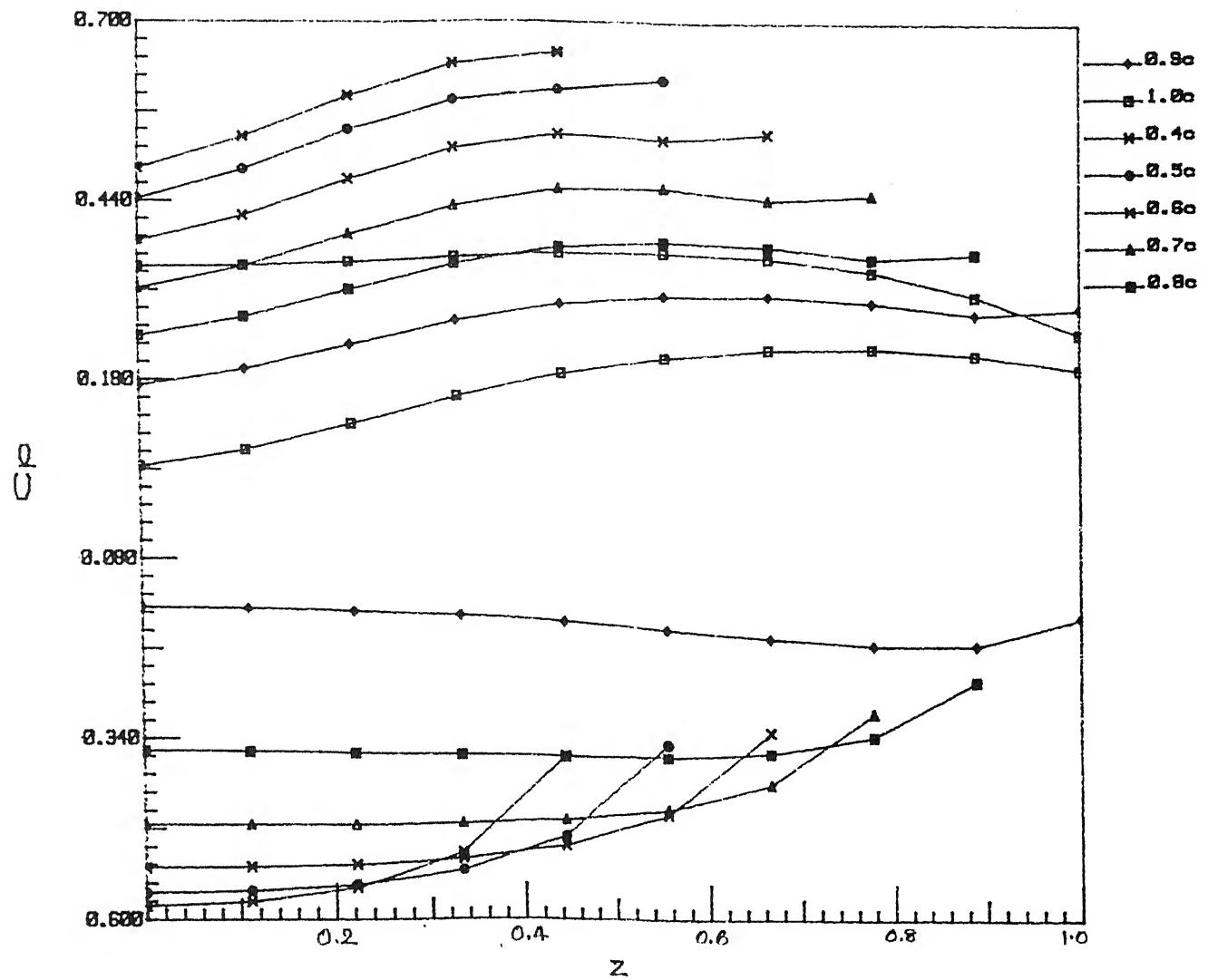
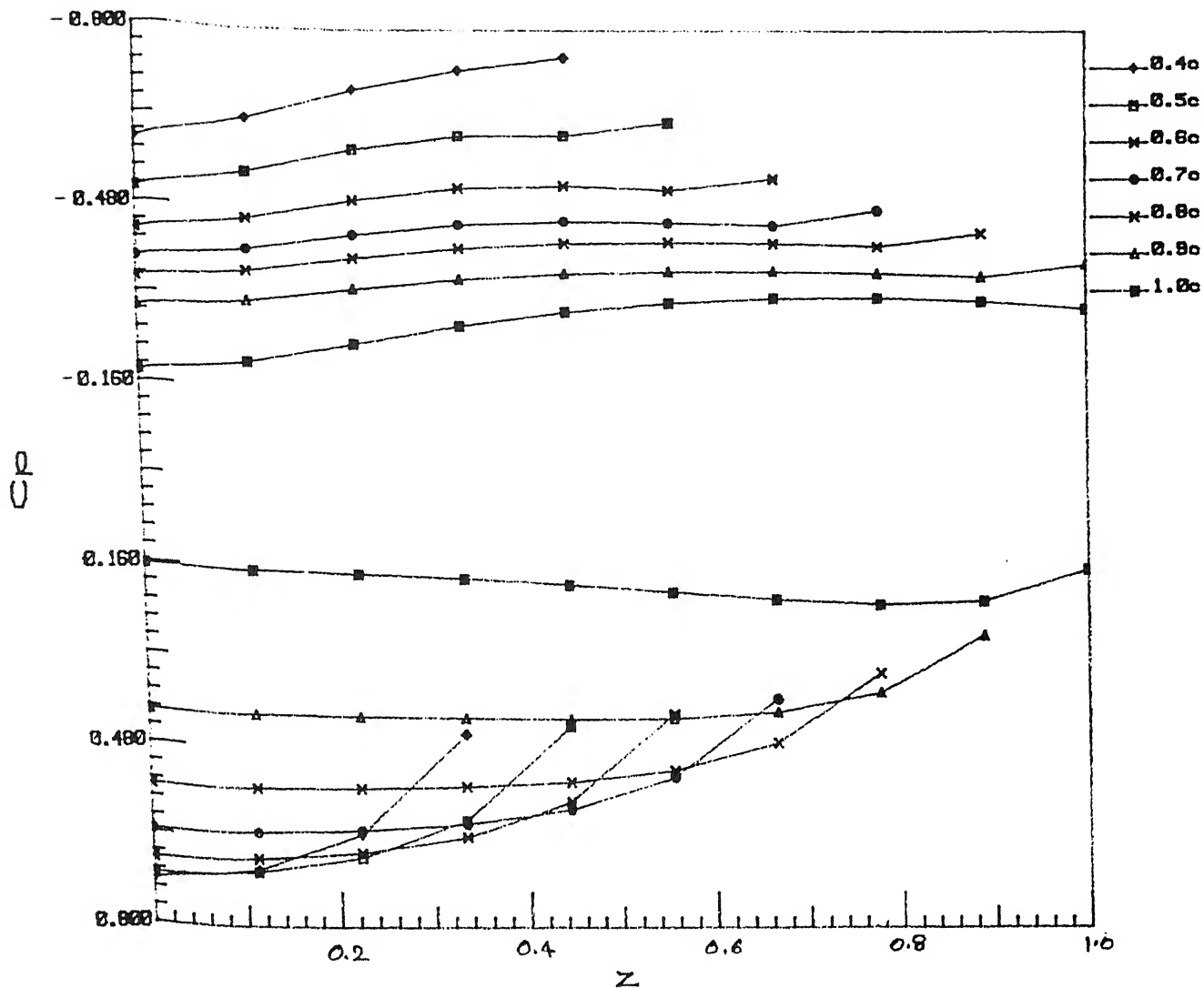
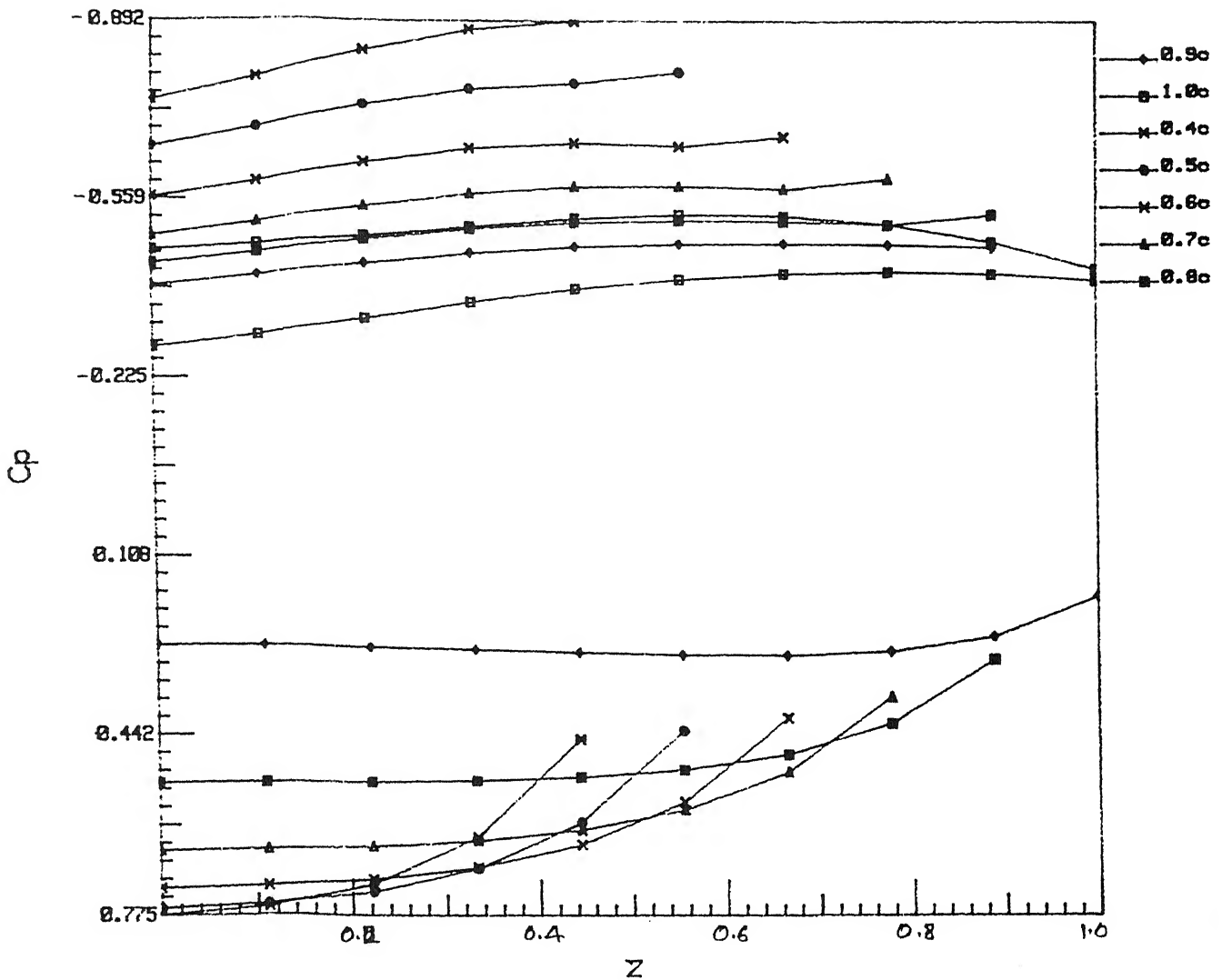


Figure 4.10: Pressure contours at different axial locations ($\alpha = 40$)

Figure 4.11: Coefficient of pressure distribution ($\alpha = 20.5$)

Figure 4.12: Coefficient of pressure distribution ($\alpha = 25$)

Figure 4.13: Coefficient of pressure distribution ($\alpha = 30$)

Figure 4.14: Coefficient of pressure distribution ($\alpha = 35$)

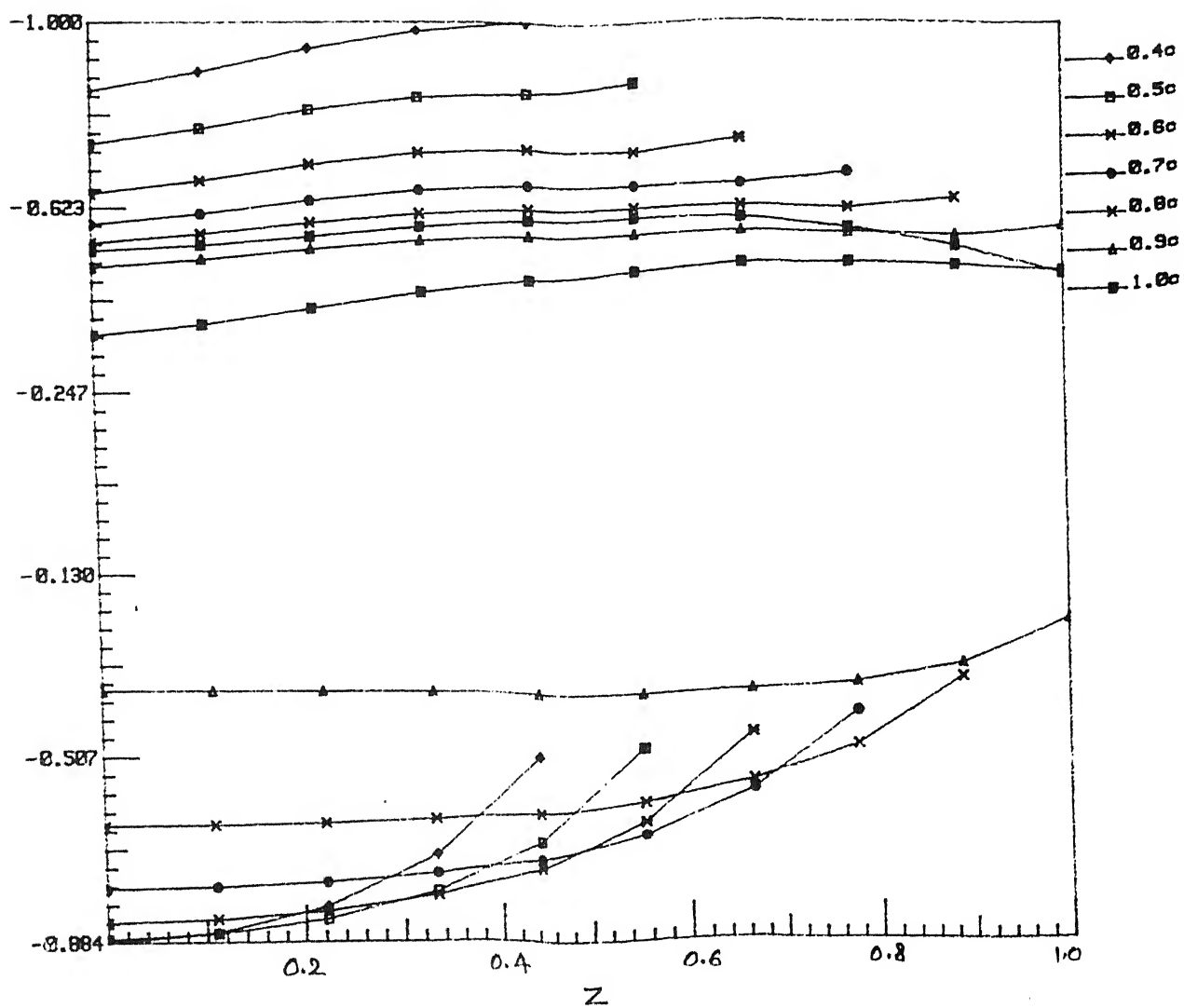


Figure 4.15: Coefficient of pressure distribution ($\alpha = 40$)

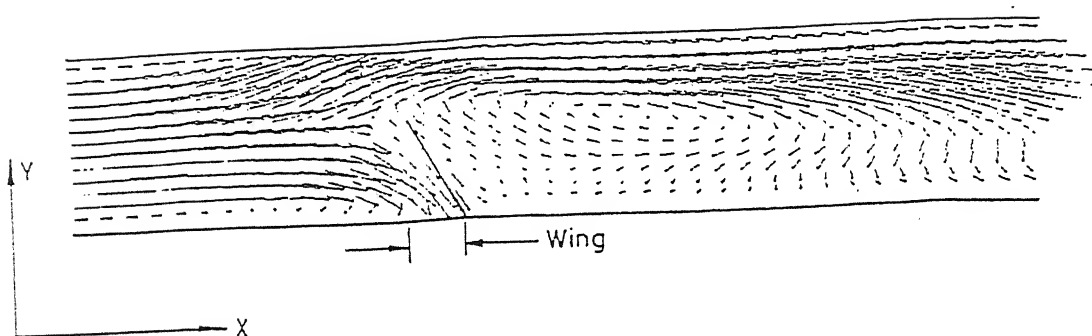
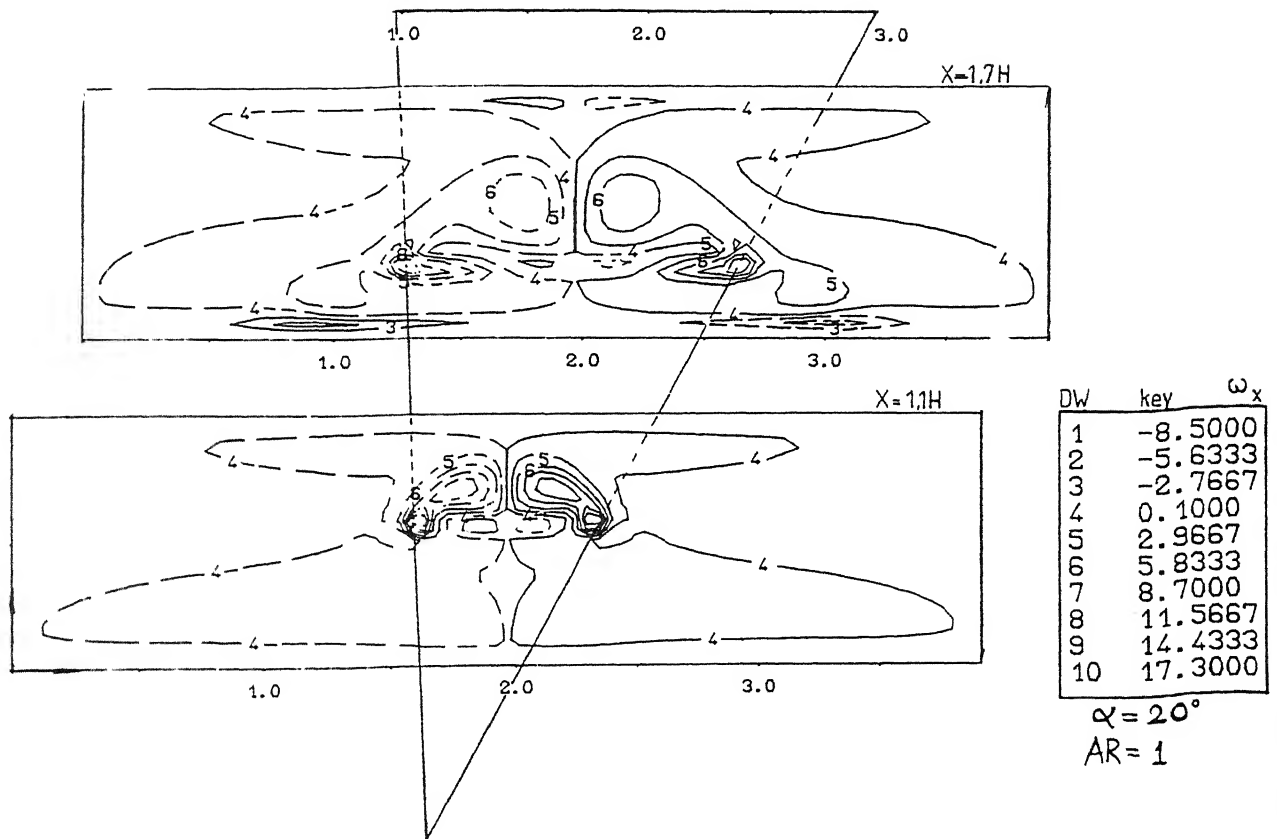


Figure 4.16: Vortex breakdown on Delta Wing (computational results) ($\alpha = 60^\circ$)

Figure 4.17: Vorticity contour ($Re = 1000$)

REFERENCES

- Angrand, F., Billey, V., Derevieux, A., Periaux, J., Pouletty, C. and Stoufflet, B., 1985, 2-D and 3-D Euler Flow Calculations with a Second-Order Accurate Galerkin Finite Element Method, *AIAA* paper 85-1706.
- Betz, A., 1935, Applied Airfoil Theory, in *Aerodynamic Theory*, vol. IV, Durand, W. F. (editor), pp. 69-72.
- Biswas, G., 1993, *Personal communication*.
- Brandt, A., Dendy, J. E. and Ruppel, H., 1980, The Multigrid Method for Semi-Implicit Hydrodynamic Codes, *J. Comp. Phy.*, vol. 34, pp. 348-370.
- Brown, C. E. and Michael, W. H. Jr., 1955, On Slender Delta Wings with Leading-Edge Separation, *NACA* TN 3430.
- Brunnenstuhl, U. and Hummel, D., 1982, Vortex Formation over Delta Wings, *ICAS* Paper 82-6.6.3, pp. 1133-1146.
- Earnshaw, P. B., 1962, An Experimental Investigation of the Structure of a Leading-Edge Vortex, *ARC R&M*, no. 3281. 3
- Eriksson, L. E. and Rizzi, A., 1984, Computation of Vortex Flow Around a Canard-Delta Combination, *Journal of Aircraft*, vol. 21, no. 11, pp. 858-865.
- Fink, P. T., 1956, Wind Tunnel Tests on a Slender Delta Wing at High Incidence, *Flugwiss*, vol. 4, pp. 247-249.

- Fink, P. T. and Taylor, J., 1967, Some Early Experiments on Vortex Separation, *ARC R&M*, no. 3489.
- Gloss, B. B. and Washburn, K. E., 1978, Load Distribution on a Close-Coupled Wing Canard at Transonic Speeds, *Journal of Aircraft*, vol. 15, no. 4, pp. 234-239.
- Gordon, R., 1990, Numerical Simulation of Vortical Flows over a Strake Delta Wing and a Close Coupled Delta-Canard Configuration, *AIAA Paper 90-3002*.
- Harlow, F. H., and Welch, J. E., 1965, Numerical Calculation of Time Independent Viscous Incompressible Flow of Fluids with Free Surfaces, *The Phy. Fluids*, vol. 8, pp. 2182-2188.
- Hess, J. L., 1975, Review of Integral Equation Techniques for Solving Potential Flow Problems with Emphasis on the Surface-Source Method, *Computer Methods in Applied Mechanics and Engineering*, vol. 5, pp. 145-196.
- Hess, J. L. and Smith, A. M. O., 1966, Calculation of Potential Flow About Arbitrary Bodies, *Progress in Aeronautical Sciences*, vol.8, pp. 1-138.
- Hirt, C. W., and Cook, J. L., 1972, Calculating Three Dimensional Flows around Structures and over Rough Terrains, *Journal of Comp. Phy.*, vol. 10, pp. 324-340.
- Hirt, C. W., Nicholas, B. D., and Romero, N. C., 1975, SOLA- A Numerical Solution Algorithm for Transient Fluid Flows, *LA-5852, Los Alamos Scientific Laboratory Report*.

- Hsu, C. H. and C. H. Liu, 1992, Numerical Study of Vortex Dominated Flows for Wings at High Incidence and Sideslip, *Journal of Aircraft* vol. 29, No. 3, pp.
- Hummel, D., 1979, On the Vortex Formation Over a Slender Wing at Large Incidence, *AGARD*, CP-247, Paper 15.
- Jameson, A., Schmidt, W. and Turkel, E., 1981, Numerical Solutions of the Euler Equations by Finite Volume Methods Using Runge- Kutta Time-Stepping Schemes, *AIAA* Paper 81-1259.
- Lamar, J. E., 1968, A Modified Multhopp Approach for Predicting Lifting Pressure and Camber Shape for Composite Planforms in Subsonic Flow, *NASA TN D-4427*.
- Legendre, R., 1952, Ecoulement au Voisinage de la Pointe avant d'un ail à forte flèche aux incidents moyennes, *ONERA Rech. Aeron.*, No. 30, Nov.-Dèc., pp. 3-8.
- Mangler, K. W. and Smith, J. H. B., 1959, A Theory of Slender Wings with Leading Edge Separation, *Proc. Royal Soc. London*, Series A, vol. 251, pp. 200-217.
- Multhopp, H., 1950, Method for Calculating the Lift Distribution of Wings (Subsonic Lifting-Surface Theory), *A. R. C. R&M no. 2884*.
- Peraire, J., Vahadi, M., Morgan, K. and Zienkiewicz, O. C., 1987, Adaptive Remeshing for Compressible Flow Computations, *Journal of Computational Physics*, vol. 72, no. 2, pp. 449-466.

Polhamus, E. G., 1966, A Concept of the Vortex Lift of Sharp Edge Delta Wings Based on a Leading Edge Suction Analogy, *NASA TN-D-3767*.

Raj, P., sikora, J. S. and Keen, J. M., 1986, Free Vortex Flow Simulation using a Three-dimensional Euler Aerodynamic Method, *ICAS* paper 86-1.5.2, pp. 604-617. Also *J. of Aircraft*, vol. 25, no. 2, 1988, pp. 128-134.

Rehbach, C., 1973, Calcul D'écoulements autour D'ailes sans Epaisseur avec Nappes Tourbillonnaires Evolutives. *La Rech. Aerosp.* no. 1973-2, pp. 53-61.

Rehbach, C., 1976, Numerical Investigation of Leading-Edge Vortex for Low Aspect-Ratio Thin Wings, *AIAA J.* vol. 14, pp. 253-255.

Rizzi, A. and Eriksson, L. E., 1984, Computation of Flow around Wings based on Euler Equations, *Journal of Fluid Mechanics*, vol. 148, pp. 45-71.

Thomas, J. L., Krist, S. T. and Anderson, W. K., 1990, Navier-Stokes Computations of Vortical Flows over Low Aspect Ratio Wings, *AIAA Journal*, vol. 28, no. 2, pp. 205-212.

Thomas, J. L. and Newsome, R. W., 1989, Navier-Stokes Computations of Lee-Side Flows over Delta Wings, *AIAA J.*, vol. 27, no. 12, pp. 1673-1679.

Vicelli, A., J., 1971, A Computing Method for Incompressible Flows bounded by Moving Walls, *J. Comp. Phys.*, vol. 8, pp. 119-143.

Volpe, G., Siclari, M. J. and Jameson, A., 1987a, Computation of Aircraft Flow Field by a Multigrid Euler Method, *AIAA*, paper 87-2268, pp. 1-13.

Volpe, G., Aiclari, M. J. and Jameson, A., 1987b, A new Multigrid Euler Method for fighter type configurations, *AIAA*, paper 87-1160, pp. 627-646.

Weber, J. A., Brune, G. W. and Forrester, T. J., 1976, Three- Dimensional Solution of Flow over Wings with Leading-Edge Separation, *AIAA J.*, vol. 14, no. 4, 1976.

Wentz, W. H. and McMahon, M. C., 1966, An Experimental of the Flow Fields about Delta and Double-Delta Wings at Low Speeds, *NASA*, CR 521.

Werle, H., 1960, *ONERA Rech. Aeron.* no. 74, pp. 23-30.